JOURNAL OF THE AMERICAN CHEMICAL SOCIETY

Subscriber access provided by BIU Pharmacie | Faculté de Pharmacie, Université Paris V

Article

Decelerating Charge Recombination Using Fluorinated Porphyrins in N,N-bis(3,4,5-trimethoxyphenyl)aniline – Aluminum(III) Porphyrin – Fullerene Reaction Center Models

Niloofar Zarrabi, Sairaman Seetharaman, Subhajyoti Chaudhuri, Noah Holzer,
Victor S. Batista, Art van der Est, Francis D'Souza, and Prashanth K Poddutoori

J. Am. Chem. Soc., **Just Accepted Manuscript** • DOI: 10.1021/jacs.0c01574 • Publication Date (Web): 28 Apr 2020

Downloaded from pubs.acs.org on April 28, 2020

Just Accepted

“Just Accepted” manuscripts have been peer-reviewed and accepted for publication. They are posted online prior to technical editing, formatting for publication and author proofing. The American Chemical Society provides “Just Accepted” as a service to the research community to expedite the dissemination of scientific material as soon as possible after acceptance. “Just Accepted” manuscripts appear in full in PDF format accompanied by an HTML abstract. “Just Accepted” manuscripts have been fully peer reviewed, but should not be considered the official version of record. They are citable by the Digital Object Identifier (DOI®). “Just Accepted” is an optional service offered to authors. Therefore, the “Just Accepted” Web site may not include all articles that will be published in the journal. After a manuscript is technically edited and formatted, it will be removed from the “Just Accepted” Web site and published as an ASAP article. Note that technical editing may introduce minor changes to the manuscript text and/or graphics which could affect content, and all legal disclaimers and ethical guidelines that apply to the journal pertain. ACS cannot be held responsible for errors or consequences arising from the use of information contained in these “Just Accepted” manuscripts.

is published by the American Chemical Society. 1155 Sixteenth Street N.W., Washington, DC 20036

Published by American Chemical Society. Copyright © American Chemical Society. However, no copyright claim is made to original U.S. Government works, or works produced by employees of any Commonwealth realm Crown government in the course of their duties.

Decelerating Charge Recombination Using Fluorinated Porphyrins in *N,N*-bis(3,4,5-trimethoxyphenyl)aniline – Aluminum(III) Porphyrin – Fullerene Reaction Center Models

Niloofar Zarrabi,[a] *Sairaman Seetharaman,*[b] *Subhajyoti Chaudhuri,*[c] *Noah Holzer,*[a] *Victor S. Batista,**[c] *Art van der Est,**[d] *Francis D'Souza,**[b] *Prashanth K. Poddutoori**[a]

[a]Department of Chemistry & Biochemistry, University of Minnesota Duluth, 1038 University Drive, Duluth, Minnesota 55812, United States. [b]Department of Chemistry, University of North Texas, 1155 Union Circle, # 305070, Denton, Texas 76203-5017, United States. [c]Department of Chemistry, Yale University, P.O. Box 208107, New Haven, Connecticut 06520-8107, United States. [d]Department of Chemistry, Brock University, 1812 Sir Isaac Brock Way, St. Catharines, ON, L2S 3A1, Canada.

ABSTRACT. In supramolecular reaction center models, the lifetime of the charge-separated state depends on many factors. However, little attention has been paid to the redox potential of the species that lie between the donor and acceptor in the final charge separated state. Here, we report on a series of self-assembled aluminum porphyrin-based triads that provide a unique opportunity to study the influence of the porphyrin redox potential independently of other factors. The triads, BTMPA-Im→AlPorF$_n$-Ph-C$_{60}$ (n = 0, 3, 5), were constructed by linking the fullerene (C$_{60}$) and bis(3,4,5-trimethoxyphenyl)aniline (BTMPA) to the aluminum(III) porphyrin. The porphyrin (AlPor, AlPorF$_3$ or AlPorF$_5$) redox potentials are tuned by substitution of phenyl (Ph), 3,4,5-trifluorophenyl (PhF$_3$) or 2,3,4,5,6-pentafluorophenyl (PhF$_5$) groups in its meso positions. The C$_{60}$ and BTMPA units are bound axially to opposite faces of the porphyrin plane *via* covalent and coordination bonds, respectively. Excitation of all of the triads results in sequential electron transfer that generates the identical final charge separated state, BTMPA$^{\bullet+}$-Im→AlPorF$_n$-Ph-C$_{60}$$^{\bullet-}$, which lies energetically 1.50 eV above the ground state. Despite the fact that the radical pair is identical in all of the triads, remarkably, the lifetime of BTMPA$^{\bullet+}$-Im→AlPorF$_n$-Ph-C$_{60}$$^{\bullet-}$ radical pair was found to be very different in each of them, that is, 1240, 740 and 56 ns for BTMPA-Im→AlPorF$_5$-Ph-C$_{60}$, BTMPA-Im→AlPorF$_3$-Ph-C$_{60}$ and BTMPA-Im→AlPor-Ph-C$_{60}$, respectively. These results clearly suggest that the charge recombination is an activated process that depends on the midpoint potential of the central aluminum(III) porphyrin (AlPorF$_n$).

INTRODUCTION

The generation of long-lived high-energy charge-separated states is an essential component of the conversion of sunlight energy into chemical energy in natural photosynthesis.[1–4] To achieve energy conversion with a high quantum yield, the photosynthetic systems use a series of electron transfer reactions along a chain of redox active cofactors. The sunlight energy collected by the light harvesting antenna systems is funneled to the reaction center complex where an extremely fast and highly efficient initial charge separation occurs. The charge separation is then stabilized by a series of secondary electron transfer steps that ultimately generate species that are long lived enough to allow oxidation and reduction of soluble donors and acceptors to occur on opposite sides of the photosynthetic membrane. In oxygenic photosynthesis, this process generates the energy-rich compounds ATP, NADPH and O_2 that are used to drive respiration, carbon fixation and a host of other biochemical processes. Mimicking the initial steps of photosynthetic energy conversion by using synthetic models is important to further our understanding of the intricate details of electron transfer process in natural photosynthesis. Most importantly, research in this area holds promise for technological advances in solar energy conversion and storage for future energy needs.[5–13] In this regard, many reaction center models have been designed and studied to mimic the photoinduced charge separation of natural systems.[9,10,14–25] However, unlike the reaction centers, charge recombination is an important factor because the number of donors and acceptors is smaller, and the complexes are not embedded in a membrane protein. In these model systems, the rate of charge separation and recombination has been studied as a function of the driving force,[26–28] reorganization energy,[29–32] and electronic coupling,[33,34] which depend on the distance between donor and acceptor units,[30,35,36] the bridge and medium connecting them,[37–39] molecular conformation,[32,40] etc. By optimizing these factors through careful design of the complexes, sequential charge transfer yielding the desired long-lived charge separated states are achieved.[41–44]

In many of these synthetic models, substituted porphyrin compounds are used because they share similar structural, physical and chemical properties with the chlorophyll chromophores of the natural photosystems.[45,46] In the artificial complexes, porphyrins are covalently or non-covalently connected to variety of redox active units. In most cases, the donor and acceptor centers are connected to the periphery of the porphyrin ring either through the meso- or pyrrolic (β-) positions. This strategy results in complexes in which the charge separation occurs in the porphyrin plane and is sometimes referred to as horizontal electron transfer. A smaller number of model compounds have been studied in which "vertical" or "axial" electron transfer occurs perpendicular to the porphyrin ring.[27,30,47–60] One of the main reasons for this limitation is the use of transition metal ions in the porphyrin cavity that do not allow more than one axial unit.

The most important factor governing biological electron transfer is the electronic coupling between the donor and acceptor, which leads to the linear dependence of the logarithm of the rate on the distance as described by the Moser-Dutton relationship.[61] In molecular systems the electronic coupling depends strongly on the nature of the bonding and the arrangement of the orbitals involved in the electron transfer. Therefore, it is fundamentally important to consider the axial arrangement as an alternative to the more common horizontal arrangement for the artificial model compounds. Moreover, the axial placement of the donor and acceptor units on opposite faces of the porphyrin ensures that they are spatially well separated and that unwanted interactions are minimized. With this objective recently we and others have reported several axial-bonding type reaction center models by exploiting the unique properties of the main group porphyrins.[35,62–70]

Among the main group porphyrins, aluminum(III) porphyrins are unique because they can form two different types of axial bonds: i) covalent Al—O bonds formed through condensation with carboxylic acids and alcohols to form ester and ether linkages, respectively,[71–74] and ii) Al—X coordination bonds (X = N, O) through Lewis acid-base interactions between Lewis bases such as pyridine and imidazole and the Al center.[35,64] These two types of bonding allow a wide variety of donors and acceptors to be attached on opposite faces of the porphyrin ring. Additionally, AlPor is highly fluorescent indicating that the excited singlet state lifetime is relatively long, which is advantageous if electron transfer is to take place. AlPor also has a rich redox chemistry with two reversible oxidation and reduction processes, allowing it to easily act as both an electron donor and acceptor. Furthermore, the optical and redox properties of AlPor can be tailored by introducing appropriate substituents in *meso*- or β-positions of the porphyrin ring for desired applications. The combination of these properties makes AlPor a unique candidate for constructing 'axial-bonding' type multi-component Donor-AlPor-Acceptor systems.

An important factor in determining the lifetime of the charge-separated state is the nature of the charge recombination reaction. In designing such systems, it is usually assumed that the direct recombination occurs between the radical ions of the final charge separated state and the rate is therefore determined primarily by the electronic coupling between them and to a lesser extent on their midpoint potentials and the reorganization energy. However, stepwise electron transfer or a hopping mechanism is also possible in which case the recombination depends on the energies of the intermediate states. To optimize the lifetime of the final charge separated state, it is therefore important to be able to distinguish between these possible recombination mechanisms.

Here we report three novel aluminum(III) porphyrin centered triads that allow this question to be addressed by taking advantage of the properties of aluminum(III) porphyrin. The structures of the three triads (BTMPA-Im→AlPor-Ph-C_{60}, BTMPA-Im→AlPorF$_3$-Ph-C_{60} and BTMPA-Im→AlPorF$_5$-Ph-C_{60}) are shown in Scheme 1. The aluminum(III) porphyrin acts as the primary electron donor/acceptor, fullerene is the primary/secondary electron acceptor, and the imidazole-appended bis(trimethoxyphenyl)aniline derivative (BTMPA) acts as the primary/secondary electron donor. We have selected fullerene as an electron acceptor due to its small reorganization energy for electron transfer.[75–77] As the secondary donor, we have designed a new compound consisting of: (i) electron-rich N,N-bis(3,4,5-trimethoxyphenyl)aniline (BTMPA) and (ii) the Lewis base imidazole (Im) attached to one another through a covalent linkage. The redox properties of aluminum(III) porphyrin are tuned by substitution of its meso positions with either phenyl (Ph), 3,4,5-trifluorophenyl (PhF$_3$) or 2,3,4,5,6-pentafluorophenyl (PhF$_5$) groups. The reported systems are designed in such a way that following excitation of aluminum(III) porphyrin, stepwise electron transfer along the axial direction is energetically favorable and produces an identical final radical pair, $BTMPA^{\bullet+}$-aluminum(III) porphyrin-$C_{60}^{\bullet-}$ in all cases. In these systems, the factors involving the donor BTMPA and acceptor C_{60} such as distance between them, the nature of the bridge, their contributions to the reorganization and Gibbs free energies are kept constant. Thus, this design allows the role of the central porphyrin aluminum(III) porphyrin in the charge separation and recombination dynamics to be studied independently of other factors. Such systems are rarely explored,[26,78] and to the best of our knowledge this first such system in which the charge separation and recombination in the axial direction is investigated as a function of the redox potential of the sensitizer. Time-resolved spectroscopy reveals that the triads depicted in Scheme 1 undergo light-induced multistep electron transfer. We will show that stabilization of the initial charge separation by secondary electron transfer occurs, and remarkably the stabilization as measured by the overall lifetime of the charge separation is more pronounced in those triads in which aluminum(III) porphyrin is substituted with electron withdrawing PhF_3 and PhF_5 groups which make it a better electron acceptor.

EXPERIMENTAL SECTION.

Synthesis. All chemicals, solvents and chromatographic materials were obtained from Aldrich Chemicals, Fisher Chemicals or Alfa Aesar and were used as received. The synthesis details of the precursor porphyrins 5,10,15,20-tetraphenylporphyrinatoaluminum(III) hydroxide (AlPor-OH),[35,65] 5,10,15,20-tetrakis(3,4,5-trifluorofluorophenyl)porphyrinatoaluminum(III) hydroxide (AlPorF$_3$-OH)[64,79] and their corresponding reference compounds AlPor-Ph[35,65] and AlPorF$_3$-Ph[64,79] are reported elsewhere. The precursor 5,10,15,20-tetrakis(pentafluorophenyl)porphyrin (H_2PorF$_5$) and its aluminum(III) derivative (AlPorF$_5$-OH) were synthesized using modified literature procedures,[79] for details see the Supporting Information and Scheme S1. The preparation of the dyad AlPor-Ph-C_{60} and the reference fullerene (C_{60}COOMe) has been reported previously.[65] The electron donor 4-(1H-imidazol-1-yl)-N,N-bis(3,4,5-trimethoxyphenyl)aniline (BTMPA-Im, Scheme S2), the dyads (AlPorF$_3$-Ph-C_{60} and AlPorF$_5$-Ph-C_{60}, Scheme 2) and one of the reference compounds (AlPorF$_5$-Ph Scheme S1) were prepared as described in the Supporting Information. The self-assembled dyads (BTMPA→AlPorF$_n$-Ph, n = 0, 3, 5) and triads (BTMPA→AlPorF$_n$-Ph-C_{60}, n = 0, 3, 5) were constructed by coordinating the BTMPA-Im with AlPorF$_n$-Ph and AlPorF$_n$-Ph-C_{60}, respectively, see Schemes 1 and 2. Because these self-assembled dyads and triads are formed in a solution equilibrium they cannot be isolated easily for elemental and mass analysis.

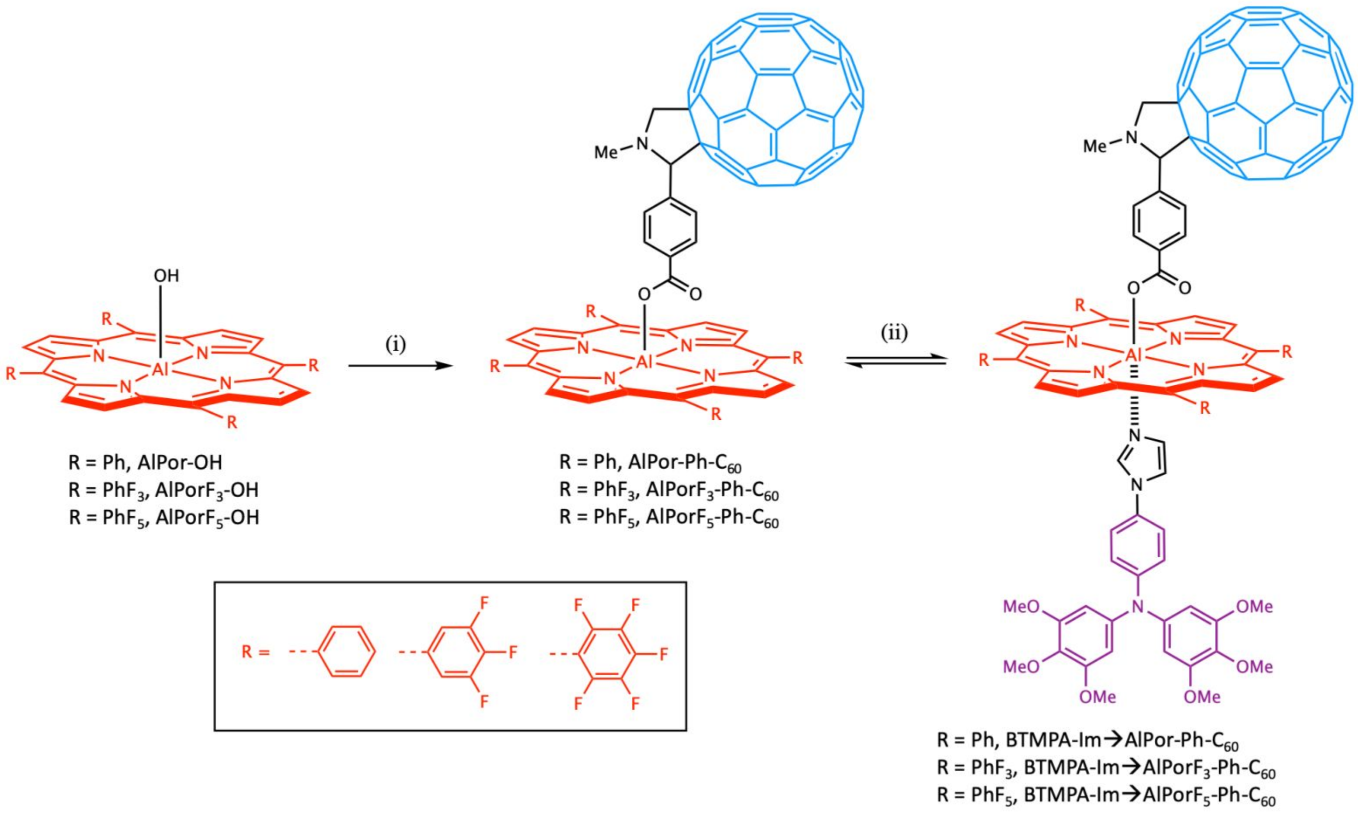

Scheme 1. Construction of the dyads AlPorF$_n$-Ph-C$_{60}$ and triads BTMPA-Im→ AlPorF$_n$-Ph-C$_{60}$, n = 0, 3, 5. Reaction conditions: (i) C$_{60}$-Ph-COOH, dry CH_2Cl_2 and CH_3OH, stirring at room temparature under nitrogen for 12-18 h. (ii) BTMAP-Im, *o*-dichlorobenzene (*o*-DCB), under titration conditions.

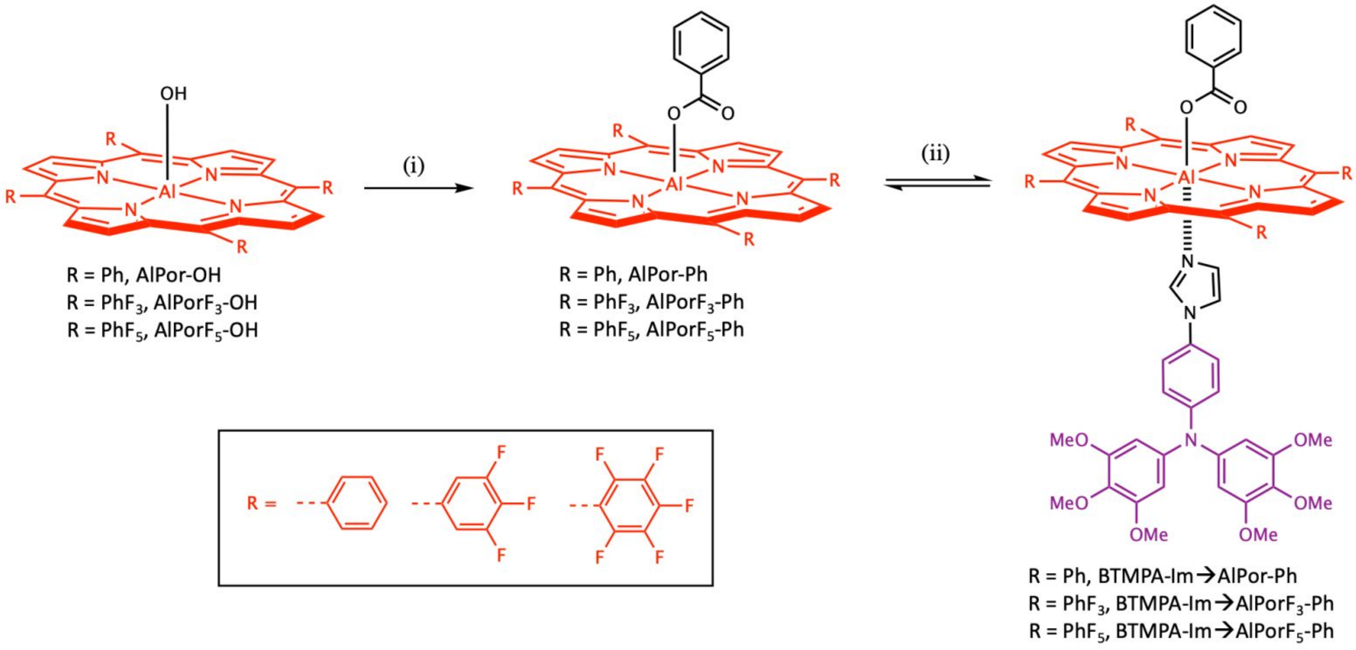

Scheme 2. Construction of the dyads BTMPA-Im→AlPorFn-Ph, n = 0, 3, 5. Reaction conditions: (i) Ph-COOH, dry CH_2Cl_2 and CH_3OH, stirring at room temparature under nitrogen for 12-18 h. (ii) BTMAP-Im, *o*-DCB, under titration conditions.

RESULTS AND DISCUSSION

Synthesis. The newly designed secondary electron donor BTMPA-Im, consisting of the electron donor BTMPA bound to the Lewis base imidazole was synthesized according to Scheme S2. The synthesis and self-assembly of dyads and triads are shown in Schemes 1 and 2. In the dyads AlPorF$_n$-Ph-C$_{60}$, fullerene is bound covalently to the porphyrin by condensation of AlPorF$_n$-OH ($n = 0, 3, 5$) with C$_{60}$-Ph-COOH in quantitative yield (see Scheme 1). The Al center in the dyad, AlPorF$_n$-Ph-C$_{60}$, acts as Lewis acid, therefore, Lewis bases such as imidazole appended *N,N*-bis(3,4,5-trimethoxyphenyl)aniline (BTMPA-Im) can be bound *via* coordination bonding through the free imidazole nitrogen to construct the supramolecular triads BTMPA$\rightarrow$AlPorF$_n$-Ph-C$_{60}$. A similar strategy was employed to construct the dyads BTMPA$\rightarrow$AlPorF$_n$-Ph starting from the reference compound AlPorF$_n$-Ph (see Figure 2).

Preliminary characterization of the covalently bound dyads and reference porphyrins was carried out by ESI High Resolution mass spectrometry. The mass spectra of the dyads and reference porphyrin showed peaks, which corresponds to the mass (*m/z*) of either $[M+H]^+$ or $[M - (PhCOO/C_{60}\text{-}PhCOO)+CH_3CN]^+$, for details see experimental section in the Supporting Information as well as Figures S1-S3. The EI mass spectra of BTMPA-Im is shown in Figure S4, and the spectra revealed $[M]^+$ peak at m/z = 491.27 (calculated 491.2056). The melting point studies indicate that all the dyads, AlPorF$_n$-Ph-C$_{60}$, and the reference compounds, AlPorF$_3$-Ph and AlPorF$_5$-Ph, are stable up to 300°C. The reference compound, AlPor-Ph and the secondary electron donor, BTMPA-Im, have melting points of 293.5-294.1°C and 166.6-168.5°C, respectively. The IR spectra of AlPor-OH, C$_{60}$-Ph-COOH, AlPor-Ph and AlPor-Ph-C$_{60}$ are shown in Figure S5. The AlPor-Ph-C$_{60}$ spectrum reveals the peaks from both AlPor and C$_{60}$ units. The absence of the carboxylic acid C=O stretching peak at 1695 cm^{-1} and presence of a characteristic C$_{60}$ vibrational mode at 527 cm^{-1} confirms formation of the dyad AlPor-Ph-C$_{60}$, i.e. C$_{60}$ is connected to AlPor through a carboxylate linker. Similar results were observed from the other two dyads, AlPorF$_3$-Ph-C$_{60}$ (Figure S6) and AlPorF$_5$-Ph-C$_{60}$ (Figure S7). The ^{1}H NMR spectra of BTMPA-Im, AlPorF$_3$-Ph-C$_{60}$ and AlPorF$_5$-Ph-C$_{60}$ are shown in Figures S8, S9 and S10, respectively. The data obtained from the spectra are summarized in the experimental section of the supporting information. The upfield shift of the bridging phenyl protons *a* and *b*, from 8.07 and 7.87 ppm in free C$_{60}$-Ph-COOH[65] to ~5.12 and ~6.80 ppm, respectively in the dyads is due to the shielding effect of the porphyrin ring current at the center of the ring and confirms axial-bonding *via* the carboxylate spacer. The protons from pyrrolidine ring appear at *c* (4.97 ppm), *d* and *e* (4.98, 4.25 ppm) and *f* (2.77 ppm) in free C$_{60}$-Ph-COOH.[65] In the dyad compounds, AlPorF$_3$-Ph-C$_{60}$ and AlPorF$_5$-Ph-C$_{60}$, these peaks were shifted upfield to ~4.77, ~4.48, ~4.00 and ~2.40 ppm, respectively. Figure S11 shows the ^{1}H NMR spectrum of a 1:1 mixture of AlPor-Ph-C$_{60}$ and BTMPA-Im (bottom) along with the individual spectra of AlPor-Ph-C$_{60}$ (middle) and BTMPA-Im (top). In the coordination complex, the shielding due to the porphyrin ring also causes an upfield shift of the BTMPA-Im protons on the imidazole unit, bridging phenyl, terminal phenyl as well as methoxy groups. The magnitude of the shift depends on the distance of the protons from the porphyrin ring and the imidazole protons display the greatest shift indicating that coordination occurs via the imidazole group. On the benzoate bridging group to the fullerene, the protons, *a*, closest to the porphyrin ring show an increased upfield shift upon coordination, suggesting that the aluminum(III) center lies out of the porphyrin plane in AlPor-Ph-C_{60} and is pulled into the plane when BTMPA-Im coordinates. Similar ^{1}H NMR titrations for AlPorF_n-Ph-C_{60} (n = 3, 5) and AlPorF_n-Ph (n = 0, 3, 5) with BTMPA-Im give analogous results (data not shown). Thus, the NMR titrations confirm the formation of the triads (BTMPA-Im$\rightarrow$AlPorF_n-Ph-C_{60}) and the dyads (BTMPA-Im$\rightarrow$AlPorF_n-Ph) in solution.

UV−visible absorption spectroscopy. The UV−visible spectra of AlPorF_3-Ph-C_{60} and its reference compounds (AlPorF_3-Ph and C_{60}-Ph-COOMe) were measured in dichloromethane (CH_2Cl_2), and the spectra are shown in Figure 1a. The band positions (Q-band and B- or Soret band) and their molar extinction coefficients are summarized in Table 1. As shown in Figure 1a, the absorption spectrum of the dyad is essentially a linear combination of its reference compounds and the positions and molar extinction coefficients (ε) of the porphyrin bands are essentially unchanged in the dyad compared to the corresponding monomer porphyrins. Similar spectral features were also observed from the dyads AlPor-Ph-C_{60} (Figure S12a) and AlPorF_5-Ph-C_{60} (Figure S12b). Overall, the absorption studies suggest that any interaction between the porphyrin (AlPorF_3) and the linked fullerene (C_{60}) is sufficiently weak that it causes no discernable change in their electronic structure. This can be attributed to their perpendicular orientation which decreases the electronic coupling between their respective π-systems. The imidazole-appended donor, BTMPA-Im, has relatively weak and very broad absorption bands in the ultraviolet region, Figure S12c.

Furthermore, the UV−visible spectra of dyads AlPorF_n-Ph-C_{60} and their reference porphyrins, AlPorF_n-Ph, were measured in *o*-dichlorobenzene (*o*-DCB), and the spectra are shown in Figure S13. The observed spectral trends and absorption profiles are consistent with CH_2Cl_2 data, although the C_{60} band in the dyads was obscured due to the solvent cutoff. The absorption bands of AlPor at 550 and 410 nm have been chosen to excite the AlPor for steady-state fluorescence and transient-absorption studies, respectively.

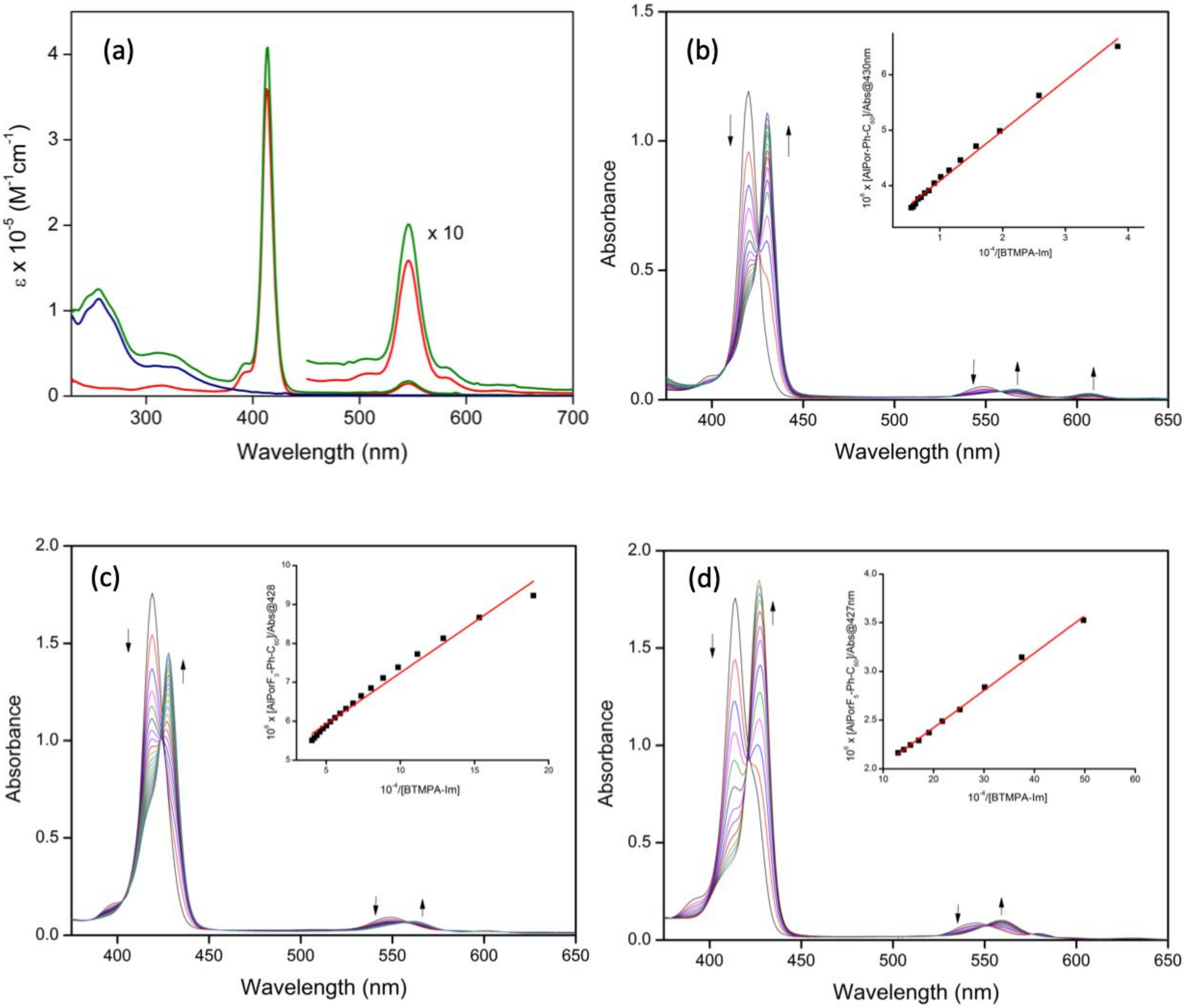

Figure 1. (a) Absorption spectra of AlPorF$_3$-Ph (red) and AlPorF$_3$-Ph-C$_{60}$ (green), C$_{60}$-Ph-COOMe (blue) in CH$_2$Cl$_2$. Absorption titrations of (b) AlPor-Ph-C$_{60}$ *vs* BTMPA-Im: BTMPA-Im was added up to 1.83×10^{-4} M in 10 μl (1.33×10^{-3} M) increments to 1 ml (4×10^{-6} M) solution of AlPor-Ph-C$_{60}$; (c) AlPorF$_3$-Ph-C$_{60}$ *vs* BTMPA-Im: BTMPA-Im was added up to 2.47×10^{-5} M in 10 μl (1.37×10^{-4} M) increments to 1 ml (4×10^{-6} M) solution of AlPorF$_3$-Ph-C$_{60}$; (d) AlPorF$_5$-Ph-C$_{60}$ *vs* BTMPA-Im: BTMPA-Im was added up to 7.69×10^{-6} M in 5 μl (1.36×10^{-4} M) increments to 1 ml (4×10^{-6} M) solution of AlPorF$_5$-Ph-C$_{60}$. All the titrations were performed in o-DCB. The inset shows the Benesi–Hildebrand plot.

Table 1. Optical and redox data of investigated compounds.

Sample	Potential [V *vs* Fc]^a Fc/Fc$^+$ = 0.84 V		Absorption^b λ_{max} [nm] (log (ε [M^{-1} cm^{-1}])) Q, B-bands & Axial Ligand Bands	Fluorescence^c λ_{max}, nm
	Oxidation	Reduction		
C_{60}-Ph-COOMe	-	−0.33, −0.73, −1.28	256 (5.06), 309 (4.55)	-
AlPor-Ph	1.22	−0.86, −1.23	547 (4.23), 416 (5.65)	596, 648
AlPor-Ph-C_{60}	1.19	−0.32, −0.70, −0.88, −1.25	548 (4.43), 416 (5.76), 255 (5.12)	595, 648
AlPorF$_3$-Ph	1.39, 1.69	−0.71, −1.09	546 (4.20), 413 (5.56)	594, 646
AlPorF$_3$-Ph-C_{60}	1.41, 1.75	−0.36, −0.73, −1.09, −1.31	546 (4.30), 414 (5.60), 256 (4.84)	593, 646
AlPorF$_5$-Ph	1.72	−0.49, −0.89	551 (4.30), 418 (5.59)	592, 648
AlPorF$_5$-Ph-C_{60}	1.70	−0.34, −0.43, −0.75, −0.95, −1.31	551 (4.36), 418 (5.59), 256 (5.05)	594, 650
BTMPA-Im	1.18	-	308 (4.95)	-

^{a}Redox potentials were reported against ferrocene, where $E_{1/2}$ (Fc/Fc$^+$) = 0.84 V with 0.1 M TBAP in *o*-DCB in our experimental conditions. ^{b}In CH_2Cl_2, ^{c}In *o*-DCB.

Axial coordination of ligands to AlPors causes a significant shift of its absorption bands. These shifts can be rationalized as arising from a change in the planarity of the porphyrin ring as the Al center, which lies above the plane of the four pyrrole nitrogen atoms in the dyad, is drawn toward the coordinating ligand. These spectral changes allow the formation of self-assembled dyads and triads (Schemes 1 and 2) to be monitored by absorption titrations, from which the binding constants can be obtained as summarized in Table S1. Figure 1b shows absorption titrations of AlPorF$_3$-Ph-C_{60} with BTMPA-Im in *o*-DCB. Upon addition of BTMPA-Im, the Soret and Q bands of the porphyrin 416, 546 and 588 nm are shifted to 422, 561 and 600 nm, which is typical of coordination of nitrogen ligands to AlPor.[66,71] Isosbestic points are observed at 426 and 555 nm, indicating the formation of the triad BTMPA-Im$\rightarrow$AlPorF$_3$-Ph-C_{60}. Benesi−Hildebrand analysis (Figure 1b, inset) gives a linear plot indicating that a 1:1 complex is formed, and the slope yields a binding constant $K = 1.7 \times 10^5$ M^{-1}. Similar spectral changes were observed in titrations of AlPor-Ph-C_{60} *vs* BTMPA-Im (Figure 1c) and AlPorF$_5$-Ph-C_{60} *vs* BTMPA-Im (Figure 1d) confirming the formation of the triads BTMPA-Im$\rightarrow$AlPor-Ph-C_{60} and BTMPA-Im$\rightarrow$AlPorF$_5$-Ph-C_{60}, respectively. The binding constants differ for the triads and follow the order: *K*(AlPor-Ph-C_{60} *vs* BTMPA-Im) < *K*(AlPorF$_3$-Ph-C_{60} *vs* BTMPA-Im) < *K*(AlPorF$_5$-Ph-C_{60} *vs* BTMPA-Im). The trend is consistent with the expected increase in the Lewis acidity of the Al center as an increasing number of fluorine atoms are added to the phenyl substituents. Hence, the Al center is the strongest Lewis acid when the porphyrin is substituted with PhF$_5$ and weakest with Ph. Therefore, it binds the Lewis base most strongly in the PhF$_5$ substituted porphyrin and most weakly with Ph substituents.

Additional titrations were carried out to establish the formation of the dyads BTMPA-Im$\rightarrow$AlPorF$_n$-Ph (n = 0, 3, 5): AlPor-Ph *vs* BTMPA-Im (Figure S14a), AlPorF$_3$-Ph *vs* BTMPA-Im (Figure S14b) and AlPorF$_5$-Ph *vs* BTMPA-Im (Figure S14c). The observed spectral changes were similar to those of the corresponding triads; thus, they establish the formation of dyads BTMPA-Im$\rightarrow$AlPorF$_n$-Ph. Furthermore, titrations of AlPorF$_n$-Ph-C_{60} (n = 0, 3, 5) with Me-Im (Figures S15) and AlPorF$_n$-Ph (n = 0, 3, 5) with Me-Im (Figures S16), were performed in *o*-

DCB, (Me-Im = 1-methylimidazole). The spectral trends are consistent with thier corresponding dyads and triads and were employed as controls in analyzing the excited state properties of the investigated systems. Together with the NMR and absorption titrations, formation of the triads BTMPA-Im→AlPorF$_n$-Ph-C$_{60}$ (n = 0, 3, 5) and dyads BTMPA-Im→AlPorF$_n$-Ph (n = 0, 3, 5) are established in solution.

Computation. The electronic structure of the dyads and triads were studied using Density Functional Theory (DFT). All the complexes (dyads and triads) were optimized at the B3LYP[80]/def2-SVP[81] level of theory using an ultrafine grid in the *Gaussian 16*[82] software. The optimizations were performed in a CPCM[83] dielectric continuum solvent model of dichlorobenzene as implemented in *Gaussian 16*. Figures 2 and S17-S19 show optimized geometries and frontier orbitals of the triads and dyads (plotted with isovalue 0.04). The DFT calculations revealed that the location of the frontier orbitals is sensitive to the *meso*-substitutions of the porphyrin.

BTMPA-Im→AlPor-Ph-C$_{60}$: As shown in Figure 2, the HOMO, LUMO, and HOMO-1 are mainly localized on the AlPor, C$_{60}$ and BTMPA moieties. However, the HOMO and HOMO-1 are significantly delocalized on to the BTMPA-Im and AlPor, respectively. Figure S19 shows the optimized geometries of one of the reference dyad BTMPA-Im→AlPor-Ph and it revealed similar delocalization of its frontier orbitals. Figure S17 shows another reference dyad, AlPor-Ph-C$_{60}$, and as projected the HOMO and LUMO are localized on the AlPor and C$_{60}$ units, respectively. Based on these results it clear that there exist strong electronic interactions between the AlPor and BTMA-Im units in the triad BTMPA-Im→AlPor-Ph-C$_{60}$ but not between AlPor and C$_{60}$ in the AlPor-Ph-C$_{60}$ dyad. The calculated radii are found to be 5.62, 8.85 and 3.50 Å for BTMPA, AlPor, and C$_{60}$, respectively. The center-to-center distance between BTMPA and C$_{60}$, BTMPA and AlPor and between AlPor and C$_{60}$ were measured to be 21.4, 9.6 and 12.4 Å, respectively. The angle between N(C$_{60}$)-N(Im)-N(BTMPA) estimated to be 157.1°.

BTMPA-Im→AlPorF$_3$-Ph-C$_{60}$: As indicated in the Figure 2, the HOMO, LUMO and HOMO-1 are localized on the BTMPA-Im, C$_{60}$ and AlPorF$_3$, respectively. Unlike the previous triad (BTMPA-Im→AlPor-Ph-C$_{60}$), the frontier orbitals in this triad are exclusively localized on their respective moieties, and therefore direct electronic interaction can be ruled out between redox centers. Moreover, the angle between N(C$_{60}$)-N(Im)-N(BTMPA) is found to be 132.9°. The decrease in the angle represents the bent geometry between BTMPA and AlPorF$_3$ units. The calculated radius for AlPorF$_3$ was found to be 9.06Å. The center-to-center distance between BTMPA and C$_{60}$, BTMPA and AlPorF$_3$ and between AlPorF$_3$ and C$_{60}$ were estimated to be 21.6, 9.5 and 12.3 Å, respectively. In the dyad BTMPA-Im→AlPorF$_3$-Ph (Figure S19), the HOMO and LUMO are restricted to the BTMPA and AlPorF$_3$ units, whereas in the dyad AlPorF$_3$-Ph-C$_{60}$ (Figure S17), the HOMO-1 and LUMO are on the AlPorF$_3$ and C$_{60}$ units, respectively.

BTMPA-Im→AlPorF$_5$-Ph-C$_{60}$: The HOMO and LUMO are localized on BTMPA-Im and C$_{60}$, respectively, see Figure 2. The electron withdrawing effect of the pentafluorinated phenyl substituents on the porphyrin lowers the energy of the highest occupied π-orbital of the porphyrin so that it lies below the HOMO-1. Again, the frontier orbitals in this system are also exclusively localized on their respective moieties, and therefore no electronic interaction can be anticipated between redox centers. Moreover, the angle between N(C$_{60}$)-N(Im)-N(BTMPA) found to be 132.9° which is same as for the BTMPA-Im→AlPorF$_3$-Ph-C$_{60}$. The HOMO and LUMO in one of the reference dyads, BTMPA-Im→AlPorF$_5$-Ph (Figure S19), are confined to the BTMPA and AlPorF$_5$, respectively. In the second reference dyad, AlPorF$_5$-Ph-C$_{60}$ (Figures S17 and S18), the HOMO-5, and LUMO are on the AlPorF$_5$ and C$_{60}$ units, respectively. The calculated radius for AlPorF$_5$ and the center-to-center distance between BTMPA and C$_{60}$, BTMPA and AlPorF$_5$ and between AlPorF$_5$ and C$_{60}$ were found to be 9.07, 21.6, 9.4 and 12.3 Å, respectively.

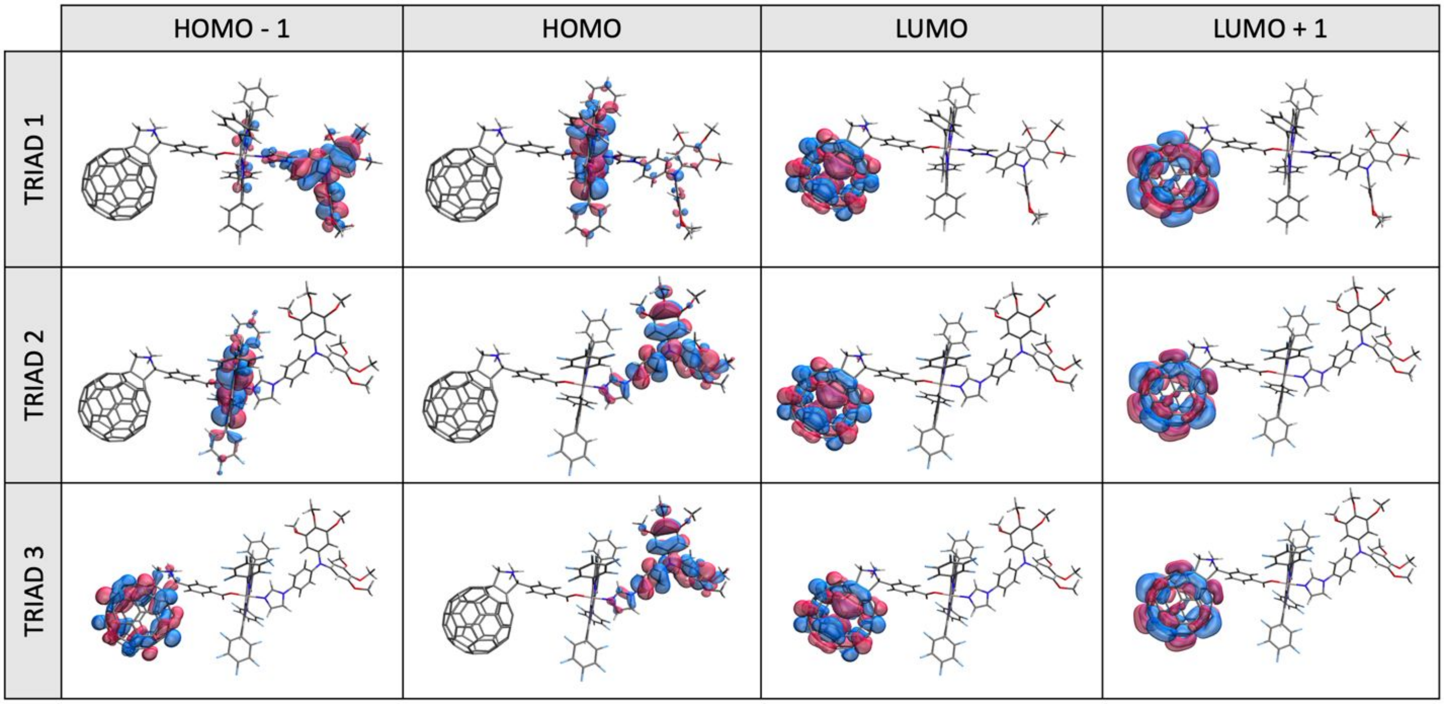

Figure 2. Frontier orbitals of BTMPA-Im→AlPor-Ph-C$_{60}$ (Triad 1), BTMPA-Im→AlPorF$_3$-Ph-C$_{60}$ (Triad 2), and BTMPA-Im→AlPorF$_n$-Ph-C$_{60}$ (Triad 3).

Energetics of dyads and triads. Cyclic voltammetry measurements of the newly synthesized compounds were performed in *o*-DCB with 0.1 M tetrabutylammonium perchlorate (TBA.ClO$_4$) as supporting electrolyte and ferrocene as an internal standard. The cyclic voltammogram of AlPor-Ph-C$_{60}$ and its reference compounds AlPor-Ph and fullerene derivative (C$_{60}$-Ph-COOMe) are reported elsewhere.[65] Representative voltammograms are shown in Figure 3, and the oxidation and reduction midpoint potentials are summarized in Table 1. The redox processes of all of the compounds are found to be one-electron reversible based on the peak-to-peak separation values, and the cathodic-to-anodic peak current ratio. During the cathodic scan, all three dyads (AlPor-Ph-C$_{60}$, AlPorF$_3$-Ph-C$_{60}$ and AlPorF$_5$-Ph-C$_{60}$) showed four reduction processes. The observed voltammograms are assigned to the combination of porphyrin and C$_{60}$ reduction processes. For the dyad AlPor-Ph-C$_{60}$, the first two processes are assigned to the reduction of C$_{60}$ and the third process to the first reduction of the porphyrin. The fourth process is a combination of the third reduction of C_{60} and the second reduction of the porphyrin. In the case of AlPorF$_3$-Ph-C_{60}, the first, third, and fourth processes are assigned to the first reduction of C_{60}, second reduction of porphyrin, and third reduction of C_{60}, respectively. Whereas, the second process is assigned to the combination of porphyrin first reduction and C_{60} second reduction. For AlPorF$_5$-Ph-C_{60}, the first reduction of porphyrin partially overlaps with the first reduction of C_{60}. The remaining distinct second, third and fourth processes are assigned to the second reduction of C_{60}, second reduction of porphyrin and third reduction of C_{60}, respectively. Comparison of the porphyrin reduction potentials in the dyads AlPorF$_n$-Ph-C_{60} and their reference compounds AlPorF$_n$-Ph shows that with increasing numbers of fluorine substituents on the phenyl groups, the porphyrin reduction potentials undergo a positive shift as a result of the increasing electron withdrawing ability of the phenyl groups.

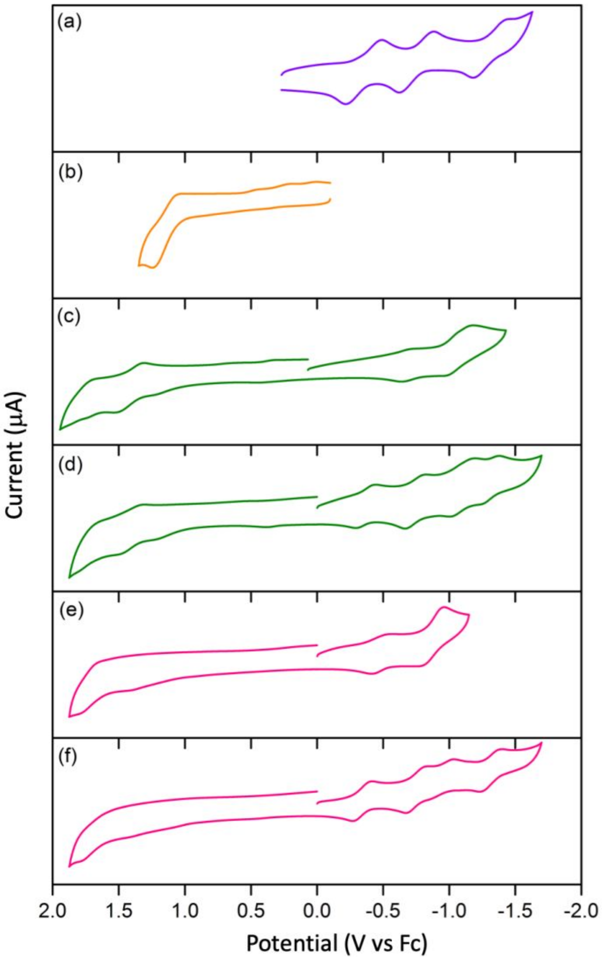

Figure 3. Cyclic voltammograms of (a) C_{60}-Ph-COOMe, (b) BTMPA-Im, (c) AlPorF$_3$-Ph, (d) AlPorF$_3$-Ph-C_{60}, (e) AlPorF$_5$-Ph and (f) AlPorF$_5$-Ph-C_{60} with 0.1 M TBA.ClO$_4$ in *o*-DCB. Voltammograms were measured with ferrocene (0.84 V *vs* Ag wire) as an internal standard. Scan rate 100 mV/s.

The anodic scan of the dyads reveals one or two oxidation processes, which are assigned to the first and second oxidation of porphyrin unit. Again, the potentials follow the same trend as the reduction potentials with a shift to more positive values as the electron withdrawing ability of the porphyrin substituents increases.

Comparison of dyads and their reference compounds show that the oxidation processes in dyads are not strongly perturbed by the addition of the fullerene. The secondary electron donor BTMPA-Im shows a one-electron process in the anodic scan corresponding to its first oxidation. Additionally, the redox potentials of the triads (physical mixtures of the dyads and BTMPA-Im) were measured to evaluate possible effects of the electron donor on the potentials of the porphyrin. The observed voltammogram (not shown) for each triad was found to be just the sum of its corresponding dyad and BTMPA-Im, which indicates that the porphyrin potentials are not perturbed by coordination of the electron donor.

The redox potentials can be used in combination with optical data to construct the energy level diagram of the states involved in possible electron-transfer processes. Figure 4 summarizes the energy levels of the investigated compounds. The energies of the lowest excited singlet states ($E_{0\text{-}0}$) of AlPor (2.14 eV), AlPorF$_3$ (2.14 eV) and C$_{60}$ (1.75 eV) and the lowest excited triplet states of AlPor (1.61 eV) and C$_{60}$ (1.55 eV) have been taken from the literature.[35,79,84] The singlet and triplet state energies of AlPorF$_3$ and AlPorF$_5$ have been calculated from their absorption and emission spectra, see Figure S20. The estimated energies are 2.14, 1.65 and 1.53 eV for ^{1}AlPorF$_5$*, ^{3}AlPorF$_3$* and ^{3}AlPorF$_5$*, respectively. The energy of the charge-separated states E_{CS} (relative to the ground state) and the free-energy changes for charge separation (ΔG_{CS}), hole stabilization (ΔG_{HS}), and electron shift (ΔG_{ES}) are estimated using the following equations 1 and 2 (also see footnotes of Table 2) and are summarized in Table 2.

$$E_{CS} = E^{ox}_{1/2}(D) - E^{red}_{1/2}(A) + G_S \tag{1}$$

Here, G_{S} is the ion-pair stabilization and incorporates both the solvent-dependent Coulomb energy change upon ion-pair formation or recombination and the free energy of solvation of the ions, Equation 2:

$$G_{\mathrm{S}} = e^2/(4\pi\varepsilon_0)[(1/(2R_+) + 1/(2R_-) - 1/R_{\mathrm{D\text{-}A}})\, 1/\varepsilon_{\mathrm{S}} - (1/(2\mathrm{R}_+) + 1/(2\mathrm{R}_-))\, 1/\varepsilon_{\mathrm{R}}] \tag{2}$$

where R_+, R_- and $R_{\mathrm{D\text{-}A}}$ are donor radius, acceptor radius and the center-to-center distance between donor and acceptor, respectively. ε_{S} is the dielectric constant of the solvent used for the photophysical studies (9.93 and 2.4 for *o*-DCB and toluene, respectively). ε_{R} is the dielectric constant of the solvent used for measuring the redox potentials, in this case *o*-DCB. Using the radii from the DFT calculations, G_{S} values of −0.15 and 0.02 - 0.06 eV are obtained for BTMPA$^{\bullet+}$-AlPorF$_n^{\bullet-}$ in *o*-DCB and toluene, respectively. For the radical ion-pairs AlPorF$_n^{\bullet+}$-Ph-C$_{60}^{\bullet-}$ in the dyads and BTMPA$^{\bullet+}$-Im$\rightarrow$AlPorF$_n$-Ph-C$_{60}^{\bullet-}$ in the triads, the calculated Coulomb stabilization due to the attraction between the cation and anion of the radical pair is small because of the relatively large R$_{\mathrm{D\text{-}A}}$ values. However, the calculated destabilization in toluene compared to *o*-DCB is unreasonably large, because of the small radius estimated for C$_{60}^{\bullet-}$. Hence for AlPorF$_n^{\bullet+}$-Ph-C$_{60}^{\bullet-}$ and BTMPA$^{\bullet+}$-Im$\rightarrow$AlPorF$_n$-Ph-C$_{60}^{\bullet-}$ we have not included the G_{S} term in their energies. Using the energies obtained from the optical and electrochemical data, the energy-level diagram was constructed for the dyads and triads in toluene (Figure 4) and *o*-DCB (Figure S21). The calculated free-energy level diagrams suggest the following electron transfer processes are energetically favorable in these triads upon excitation of AlPorF$_n$: (i) oxidative electron transfer from the excited singlet state of AlPorF$_n$ (^{1}AlPorF$_n$*) to fullerene followed by a hole shift to BTMPA, or (ii) reductive electron transfer from BTMPA to ^{1}AlPorF$_3$* followed by a charge shift to C$_{60}$. However, the rates of these processes are determined by the electronic coupling and activation energy, which depends on the reorganization energy as well as the free energy change.

Table 2. Experimentally calculated free energy change (ΔG) values of charge separation (CS) and charge recombination (CR) processes of the investigated dyads and triads in toluene.

Compound	E_{CS1}	E_{CS2}	E_{CS3}	ΔG_{CS1}	ΔG_{CS2}	ΔG_{CR}
AlPor-Ph-C$_{60}$	1.51	-	-	–0.63	-	–1.51
BTMPA-Im→AlPor-Ph	-	2.10	-	-	–0.04	–2.10
BTMPA-Im→AlPor-Ph-C$_{60}$	1.51	2.10	1.50	–0.63	–0.04	–1.50
AlPorF$_3$-Ph-C$_{60}$	1.77	-	-	–0.37	-	–1.77
BTMPA-Im→AlPorF$_3$-Ph	-	1.93	-	-	–0.21	–1.93
BTMPA-Im→AlPorF$_3$-Ph-C$_{60}$	1.77	1.93	1.52	–0.37	–0.21	–1.52
AlPorF$_5$-Ph-C$_{60}$	2.04	-	-	–0.10	-	–2.04
BTMPA-Im→AlPorF$_5$-Ph	-	1.63	-	-	–0.51	–1.63
BTMPA-Im→AlPorF$_5$-Ph-C$_{60}$	2.04	1.63	1.52	–0.10	–0.51	–1.63

CS1: AlPorF$_n^{\bullet+}$-C$_{60}^{\bullet-}$
CS2: BTMPA$^{\bullet+}$-AlPorF$_n^{\bullet-}$
CS3: BTMPA$^{\bullet+}$-AlPorF$_n$-C$_{60}^{\bullet-}$

$\Delta G_{CS} = E_{CS} - E_{0\text{-}0}$, $E_{0\text{-}0} = 2.14$ eV
$\Delta G_{CR} = -E_{CS}$

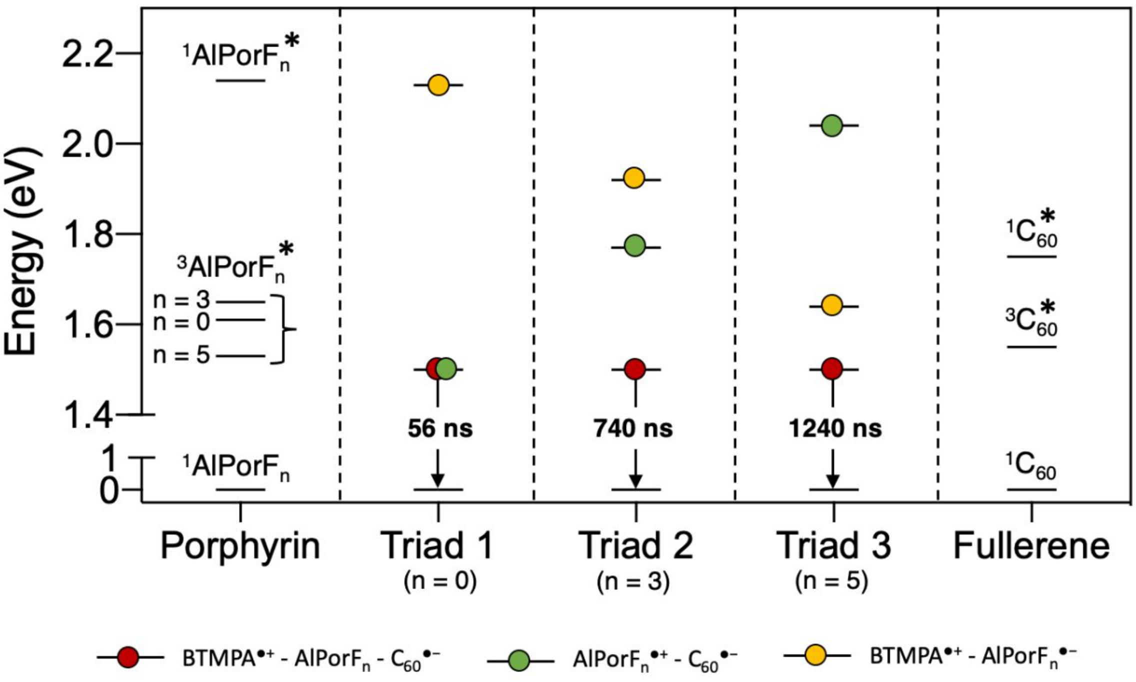

Figure 4. Energy level diagram of investigated triads BTMPA-Im→AlPorF$_n$-Ph-C$_{60}$ in toluene.

Steady-state fluorescence studies. The steady-state fluorescence spectra of the dyads and triads were measured in *o*-DCB (Figure 5) and toluene (Figure S22). Interestingly, very similar results were observed in both solvents. This is unusual because fluorescence quenching by electron transfer is typically less efficient in non-polar solvents such as toluene. The experiments were carried out at same concentration of porphyrin in all samples. The spectra were measured with an excitation wavelength of 555 nm, which excites the Q-band transition of the porphyrin.

$AlPorF_n$-Ph-C_{60}: Figure 5 shows the fluorescence spectra of the dyads AlPor-Ph-C_{60}, $AlPorF_3$-Ph-C_{60} and $AlPorF_5$-Ph-C_{60} and its reference compound AlPor-Ph, $AlPorF_3$-Ph and $AlPorF_5$-Ph, respectively in *o*-DCB, and the emission maxima are summarized in Table 1. All of the compounds exhibit two bands due to porphyrin emission. The band positions in the dyad and its reference porphyrin are very similar indicating that the electronic structure of the porphyrin is not perturbed by axial-linkage of C_{60} unit. However, the fluorescence of the porphyrin is quenched, 80%, 66% and 50%, in AlPor-Ph-C_{60}, $AlPorF_3$-Ph-C_{60} and $AlPorF_5$-Ph-C_{60}, respectively. Based on the energy level diagram, the $AlPor^{\bullet +}$-Ph-$C_{60}^{\bullet -}$, $AlPorF_3^{\bullet +}$-Ph-$C_{60}^{\bullet -}$ and $AlPorF_5^{\bullet +}$-Ph-$C_{60}^{\bullet -}$ charge separated states lie energetically below the excited singlet state of porphyrin ($^1AlPorF_n^*$), therefore the observed quenching is assigned to oxidative electron transfer from $^1AlPorF_n^*$ to C_{60}. The calculated ΔG_{CS} for this electron transfer was found to be −0.64, −0.27 and −0.10 eV for AlPor-Ph-C_{60}, $AlPorF_3$-Ph-C_{60} and $AlPorF_5$-Ph-C_{60}, respectively (see Table 2). The fact that the quenching follows the same trend as the driving force for the electron transfer suggests that electron transfer lies in the normal region of the Marcus curve as would be expected.

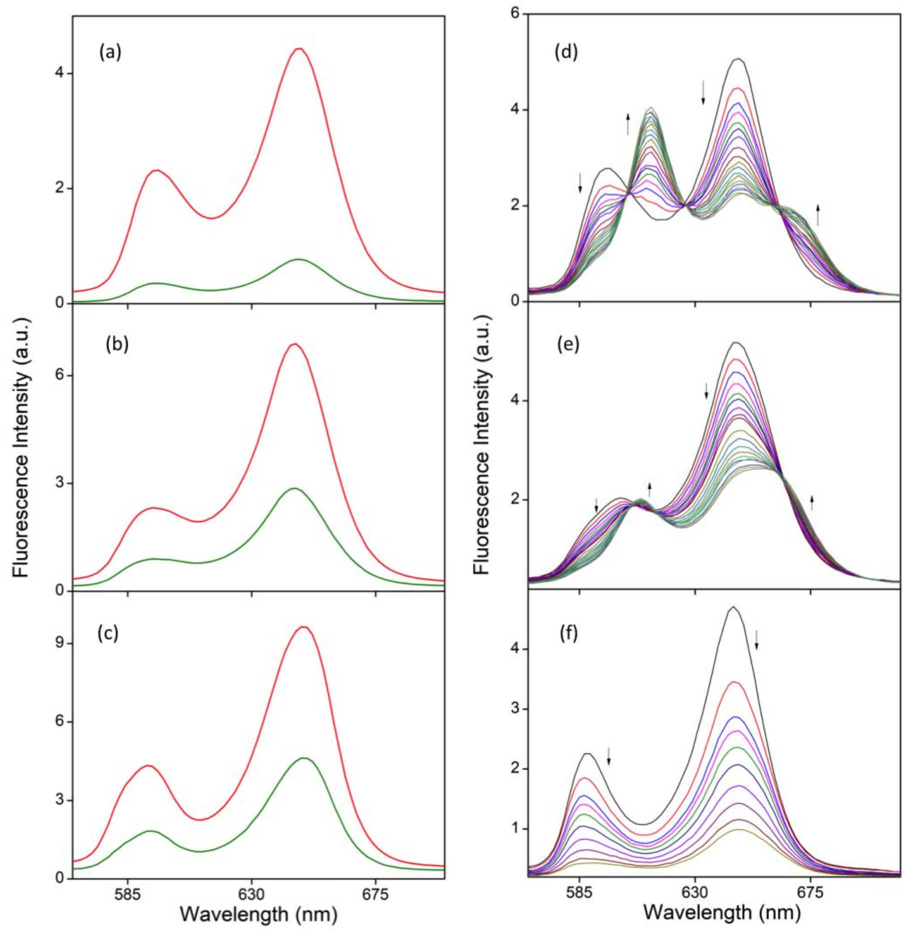

Figure 5. Fluorescence spectra of (a) AlPor-Ph (red) and AlPor-Ph-C$_{60}$ (green), (b) AlPorF$_3$-Ph (red) and AlPorF$_3$-Ph-C$_{60}$ (green), (c) AlPorF$_5$-Ph (red) and AlPorF$_5$-Ph-C$_{60}$ (green), (d) AlPor-Ph *vs* BTMPA-Im: BTMPA-Im was added up to 1.52×10^{-4} M in 10 µl (6.60×10^{-4} M) increments to a 1 ml (4×10^{-6} M) solution of AlPor-Ph, (e) AlPorF$_3$-Ph *vs* BTMPA-Im: BTMPA-Im was added up to 3.0×10^{-5} M in 10 µl (1.37×10^{-4} M) increments to a 1 ml (4×10^{-6} M) solution of AlPorF$_3$-Ph, and (f) AlPorF$_5$-Ph *vs* BTMPA-Im: BTMPA-Im was added up to 5.54×10^{-6} M in 10 µl (6.7×10^{-5} M) increments to a 1 ml (4×10^{-6} M) solution of AlPorF$_5$-Ph. All the titrations were performed in *o*-DCB.

BTMPA-Im→AlPorF$_n$-Ph: In order to establish the formation of the dyads (Scheme 2) and evaluate possible photoinduced processes between BTMPA-Im and AlPorF$_n$, steady-state fluorescence titrations were performed between BTMPA-Im and AlPorF$_n$-Ph in *o*-DCB. The excitation wavelength in each of these titrations was adjusted to the isosbestic point, which was obtained from the corresponding absorption titrations, so that the extinction coefficient is the same for each sample solution. As shown in Figure 5d, upon addition of BTMPA-Im to AlPor-Ph, the AlPor fluorescence peaks shift to longer wavelengths from 594 and 646 nm to 613 and 665 nm, respectively along with a change in their relative intensities. The observed spectral changes support the formation of the dyad BTMPA-Im→AlPor-Ph in solution. To investigate the possible reductive electron transfer between the BTMPA and AlPor, a control titration of AlPorF-Ph *vs* Me-Im (without BTMPA, Figure S23a) was performed. Spectral changes similar to those found in the titration of AlPor-Ph *vs* BTMPA-Im are observed suggesting that they are a result of the binding of the imidazole moiety and not due to the presence of BTMPA as an electron donor. Therefore, the rate of the anticipated reductive electron transfer from BTMPA to ^{1}AlPor* is negligible compared to the fluorescence rate. This is consistent with the small free energy change of –0.01 eV calculated for this process (ΔG_{CS2} in Table 2) since in this case, the activation energy for the electron transfer is determined mostly by the reorganization energy and is expected to be fairly large.

In the case of AlPorF$_3$-Ph *vs* BTMPA-Im (Figure 5e) titrations, the fluorescence bands are red shifted which again confirms the formation of the dyad BTMPA-Im→AlPorF$_3$-Ph. However, the fluorescence intensity decreases upon addition of BTMPA-Im. The corresponding control titrations AlPorF$_3$-Ph *vs* Me-Im (Figure S23b) revealed band shifts to longer wavelengths but without a change in fluorescence intensity suggesting that the fluorescence quenching during the titrations of AlPorF$_3$-Ph *vs* BTMPA-Im is indeed due to the presence of BTMPA and reductive electron transfer from BTMPA to ^{1}AlPorF$_3$*. This is also consistent with the much larger value of –0.22 eV for the ΔG_{CS2}. Figure 5c shows the titrations of AlPorF$_5$-Ph *vs* BTMPA-Im, which establish the formation of BTMPA-Im→AlPorF$_5$-Ph. A significant fluorescence quenching is exhibited without a spectral shift in presence of BTMPA-Im. In contrast, the control titrations AlPorF$_5$-Ph *vs* Me-Im (Figure S23c) show a shift of the bands but no quenching. This implies that essentially complete quenching occurs when BTMPA-Im binds and the fluorescence observed in the titration with BTMPA-Im arises only from the fraction of unbound porphyrin molecules. The observed substantial quenching is assigned to the reductive electron transfer from BTMPA to ^{1}AlPorF$_5$* and again is consistent with the larger free energy change of –0.44 eV and hence lower activation energy for this process. Overall, the observed fluorescence quenching pattern in the dyads is consistent with the expected behavior based on the Gibbs free energy values and electron transfer in the normal region of the Marcus curve.

BTMPA-Im→AlPorF$_n$-Ph-C$_{60}$: Figure S24 shows the fluorescence titrations of AlPorF$_n$-Ph-C$_{60}$ *vs* BTMPA-Im in *o*-DCB. The spectral trends are very similar to their corresponding AlPorF$_n$-Ph *vs* BTMPA-Im titrations and confirm the formation of the triad BTMPA-Im→AlPorF$_n$-Ph-C$_{60}$ in solution. The excitation of AlPorF$_n$ in the triad results in an initial charge separation either as the oxidative electron transfer from ^{1}AlPorF$_n$* to C$_{60}$ or the reductive electron transfer from BTMPA to ^{1}AlPorF$_n$*. Qualitatively, the observed spectral trends during the titrations show that degree of fluorination of the porphyrin substituents influences which of the two possible electron transfer reactions occurs. Upon addition of BTMPA-Im to AlPor-Ph-C$_{60}$ (Figure S24a) the AlPor fluorescence bands shift to longer wavelengths 613 and 665 nm without any additional quenching. By comparing these trends with control titrations, AlPor-Ph *vs* BTMPA-Im (Figure 5d) and AlPor-Ph-C$_{60}$ *vs* Me-Im (Figure S23d), it is reasonable to predict that oxidative electron transfer from ^{1}AlPor* to C$_{60}$ is the initial process in the triad BTMPA-Im→AlPor-Ph-C$_{60}$. In contrast, in the titrations of AlPorF$_3$-Ph-C$_{60}$ with BTMPA-Im (Figure S24b) the fluorescence bands are shifted to 609 and 657 nm with a moderate decrease in their intensities. In this case, comparison with control titrations of AlPorF$_3$-Ph *vs* BTMPA-Im (Figure 5e) and AlPorF$_3$-Ph-C$_{60}$ *vs* Me-Im (Figure S23e), as well as the energy level diagram (Figure 4) suggest that the observed decrease in fluorescence intensity is due to reductive electron transfer from BTMPA to ^{1}AlPorF$_3$*. This implies that the rate of reductive electron transfer rate is comparable to or faster than that of the oxidative electron transfer rate from ^{1}AlPorF$_3$* to C$_{60}$. Lastly, Figure S24c shows the fluorescence spectra of the AlPorF$_5$-Ph-C$_{60}$ with increasing amounts of BTMPA-Im. In this case, addition of BTMPA-Im, leads to strong quenching without any significant shift of the emission bands. Consistent with the control experiments, AlPorF$_5$-Ph *vs* BTMPA-Im (Figure 5f) and AlPorF$_5$-Ph-C$_{60}$ *vs* Me-Im (Figure S23f), as well as the energy diagram (Figure 4), the observed strong quenching in BTMPA-Im→AlPorF$_5$-Ph-C$_{60}$ implies that reductive electron transfer from BTMPA to ^{1}AlPorF$_5$* is the fastest process in this triad.

Spectroelectrochemistry. To help interpret the transient spectral data of the products formed during the process of charge injection, spectroelectrochemical studies were performed on AlPorF$_3$-Ph and AlPorF$_5$-Ph, and BTMPA-Im in *o*-DCB containing 0.2 M TBA.ClO$_4$. As shown in Figure S25, the oxidation of BTMPA-Im results in a decrease in absorbance at 308 nm which is accompanied by the appearance of a new peak with a maximum around 333 nm. An isosbestic point at 340 nm is also observed. The oxidation of AlPorF$_3$ revealed the appearance of new bands at 595 and 690 nm, whereas the reduction produced bands at 568 and 608 nm, Figure S26. In the case of AlPorF$_5$, the oxidation resulted in new peaks at 644 and 686 nm and reduction developed peaks at 450 and 627 nm, Figure S27. The spectroelectrochemical data of the AlPor have been reported previously[63] and show that peaks at 600 and 685 nm are formed when AlPor is oxidized and at 570 and 610 nm when it is reduced.

Femtosecond Transient Absorption Spectroscopy. Having proposed the different photochemical charge separation events in the AlPorF$_n$-Ph-C$_{60}$ dyads and BTMPA-Im→AlPorF$_n$-Ph-C$_{60}$ triads from the energy levels diagrams shown in Figure 4 and fluorescence titrations shown in Figure 5, femtosecond and nanosecond transient absorption spectral studies were performed to secure direct experimental evidence of charge separation and also to evaluate the lifetimes of the charge separated states. In the present study, we have used toluene rather than *o*-DCB as the solvent because of its better photochemical stability under laser irradiation

Figure 6 shows the femtosecond transient spectra at the indicated delay times for AlPor-Ph, AlPorF$_3$-Ph and AlPorF$_5$-Ph in the absence and presence of axial coordinating BTMPA-Im. The transient spectral features of AlPor-Ph, AlPorF$_3$-Ph and AlPorF$_5$-Ph have a similar pattern, however, with subtle differences. In the case of AlPor-Ph, the instantaneously formed ^{1}AlPor* (see the spectrum at 1 ps in Figure 6a) has positive peaks at 448, 578, 611 and 1240 nm due to transitions originating from the ^{1}AlPor* state. Negative peaks at 550, 595 and 651 nm are also observed. By comparison with the absorption and fluorescence spectral data described above, the 550 nm peak is assigned to ground state bleaching and the latter two peaks are assigned to stimulated emission. The lifetime of the decay of positive peaks and recovery of the negative peaks is longer than the 3 ns time window accessible in the experiment, which is consistent with the 7.88 ns fluorescence lifetime of AlPor, determined from time correlated single photon counting measurements. The decay and recovery of the positive and negative peaks are accompanied by new peaks emerging in the 500 and 840 nm region due to the formation of ^{3}AlPor* by intersystem crossing. In the case of AlPorF$_3$-Ph, transient positive peaks of ^{1}AlPorF$_3^*$ are observed at 453, 595 and 1236 nm while the transient negative peak at 550 nm due to ground state bleaching and at 650 nm due to stimulated emission are also observed (Figure 6d). Slow intersystem crossing populating ^{3}AlPorF$_3^*$ leads to peaks at 490 and 835 nm on a timescale consistent with the fluorescence lifetime of 3.74 ns. Finally, for AlPorF$_5$-Ph photoexcitation results in positive peaks at 454, 573, 610 and 1230 nm from the excited singlet state accompanied by negative peaks at 546, 589 and 645 nm due to ground state bleaching and stimulated emission (Figure 6g). The ^{3}AlPorF$_5^*$ state formed by intersystem crossing resulted growth of new peaks at 450 and 832 nm on a ns timescale. Again, this is consistent with the fluorescence lifetimes of 2.32 ns. In summary, AlPor-Ph, AlPorF$_3$-Ph and AlPorF$_5$-Ph all show similar behavior with instantaneous formation of the excited singlet state, which decays with a lifetime of several nanoseconds to the ground state and excited triplet state.

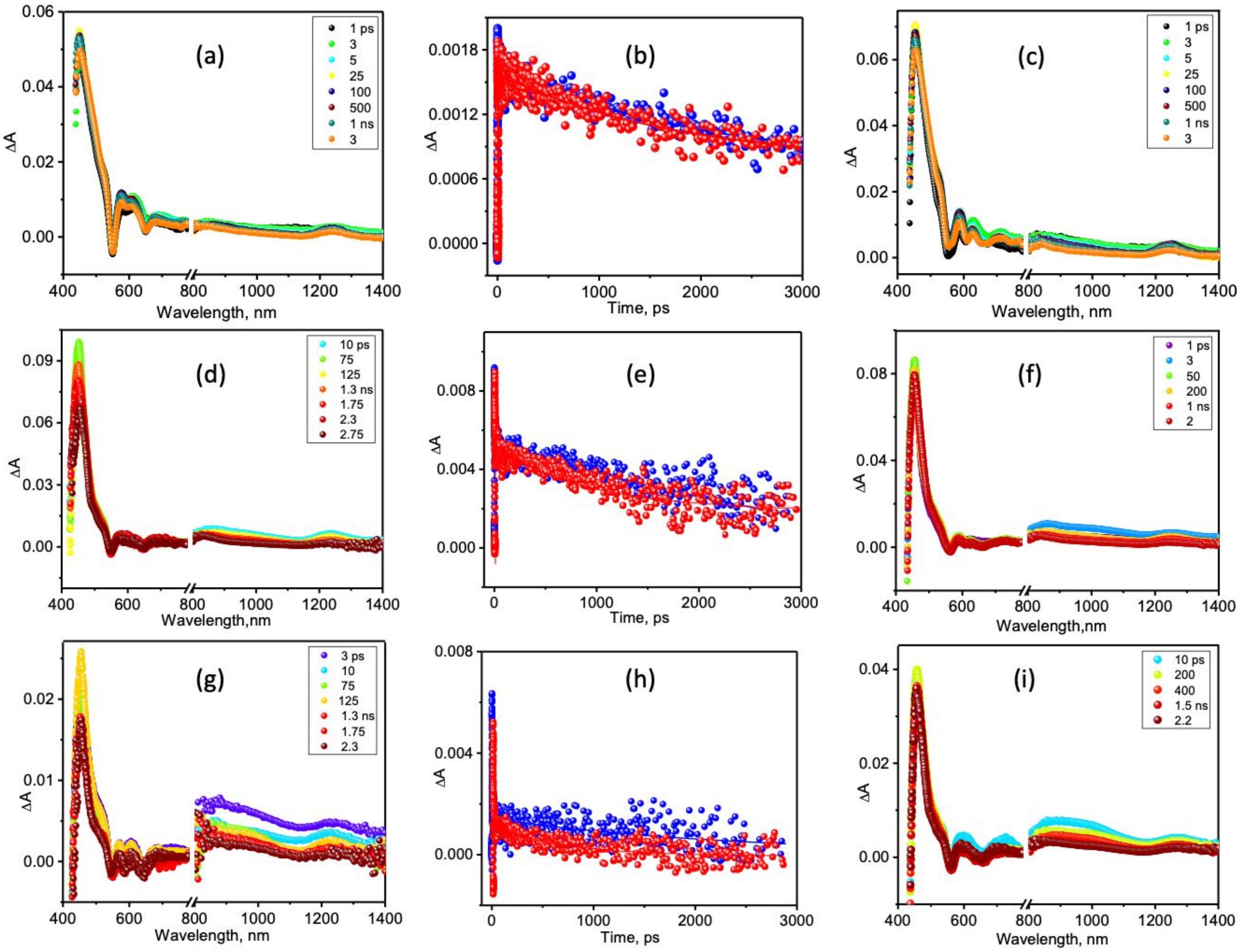

Figure 6. Femtosecond transient absorption spectra at the indicated delay times (λ_{ex} = 410 nm) of (a) AlPor-Ph, (c) BTMPA-Im→AlPor-Ph, (d) AlPorF$_3$-Ph, (f) BTMPA-Im→AlPorF$_3$-Ph, (g) AlPorF$_5$-Ph, and (i) BTMPA-Im→AlPorF$_5$-Ph in toluene. The central panel (b), (e), and (h) shows the time profile of the near-IR peak at 1240 nm in the absence (blue trace) and presence (red trace) of coordinated BTMPA to a given AlPorF$_n$-Ph.

Figure 6, panels (c), (f) and (i) show the femtosecond transient absorbance spectra of dyads BTMPA-Im→AlPor-Ph, BTMPA-Im→AlPorF$_3$-Ph, and BTMPA-Im→AlPorF$_5$-Ph. The central panels (b, e and h) show the time profiles of the near-IR peak located at 1240 nm due to singlet-singlet absorption of ^{1}AlPorF$_n$* in the presence (red) and absence (blue) of BTMPA. Upon coordination of BTMPA-Im with AlPor-Ph, positive transient peaks originating from BTMPA-Im→^{1}AlPor*-Ph are located at 452, 587, 627, 710 and 1248 nm, and negative red-shifted transient peaks at 556 nm due to ground state bleaching, and at 608 and 660 nm due to stimulated emission are observed. The energy level diagram shown in Figure 4 predicts BTMPA$^{\bullet+}$-AlPor$^{\bullet-}$ lies only 0.01 eV lower than ^{1}AlPor* thus hole transfer from the porphyrin to the donor is expected to be slow or negligent. Consistent with this, the two kinetic traces overlap in Figure 6b revealing little or no effect of BTMPA, that is, the absence of significant amounts of a hole shift leading to BTMPA$^{\bullet+}$-Im→AlPor$^{\bullet-}$-Ph. In the cases of BTMPA-Im→^{1}AlPorF$_3$*-Ph and BTMPA-Im→^{1}AlPorF$_5$*-Ph, the hole shift leading to BTMPA$^{\bullet+}$AlPorF$_3^{\bullet-}$ and BTMPA$^{\bullet+}$-AlPorF$_5^{\bullet-}$ were found to be exothermic by 0.22 and 0.44 eV, respectively. Under such conditions, new transient peaks corresponding to the charge-separated states is expected. Spectroelectrochemical studies show that BTMPA$^{\bullet+}$ has a band at 333 nm (Figure S25) while AlPorF$_3^{\bullet-}$ has bands at 568 and 608 nm (Figure S26) and AlPorF$_5^{\bullet-}$ has bands at 450 and 627 nm (Figure S27). The band at 333 nm due to BTMPA$^{\bullet+}$ is not accessible with the femtosecond setup used. The bands due to the porphyrin radical anion overlap with those of the excited singlet state or have weak intensity making it difficult to positively identify them in the femtosecond data. However, the kinetic time profiles of the 1240 nm near-IR peak provide some evidence for the expected charge separation. As shown in Figures 6e and 6h, there is an indication of a slight acceleration of the decay of both ^{1}AlPorF$_3$* and ^{1}AlPorF$_5$* in the presence of BTMPA, which might be due to the hole shift in these two dyads. From the fitted decay lifetimes, the rate constants for hole shift, k_{HS} were estimated to be 0.80×10^9 s^{-1} and 1.83×10^9 s^{-1}, respectively, for BTMPA-Im→AlPorF$_3$-Ph and BTMPA-Im→AlPorF$_5$-Ph.

Next, photoinduced charge separation in the covalently linked AlPor-Ph-C$_{60}$, AlPorF$_3$-Ph-C$_{60}$, and AlPorF$_5$-Ph-C$_{60}$ and their coordination complexes with BTMPA-Im were performed. In agreement with our earlier studies,[35,65] the femtosecond data reveal that photoexcitation of AlPor in the dyad AlPor-Ph-C$_{60}$ results in charge separation from ^{1}AlPor* to C$_{60}$ leading to the formation of AlPor$^{\bullet+}$-C$_{60}^{\bullet-}$. The absorption peak at ~450 nm, the near-IR peak at 1240 nm, and the negative peaks due to S$_1$ emission at 590 and 650 nm decayed more rapidly than in AlPor-Ph (see Figure 6a). Additionally, these processes were accompanied by new signals in the range of 600-650 nm corresponding to AlPor$^{\bullet+}$ and near 1000 nm from C$_{60}^{\bullet-}$. Since the 1000 nm peak of C$_{60}^{\bullet-}$ and 1240 nm peak of ^{1}AlPor* were far from other transient bands they can be used to estimate the rate constant for charge separation, k_{CS}. The transient spectra of BTMPA-Im→AlPor-Ph-C$_{60}$ at different delay times (Figure 7c) show peaks characteristic of the charge-separated state and provide evidence for the charge separation from ^{1}AlPor* to

C_{60}. However, the decay of the absorbance change due to $C_{60}^{\bullet-}$ at 1000 nm (Figure 7b, red trace) is longer than the 3 ns time window of our instrumental setup. Thus, in this case the rate constant for charge recombination, k_{CR} was evaluated from nanosecond transient spectral studies that will be discussed in the next section. If hole transfer from BTMPA to $AlPor^{\bullet+}$ occurs then one would expect the decay of $C_{60}^{\bullet-}$ to be slower when BTMPA is bound, that is, the larger separation of the radical cation and radical anion species in $BTMPA^{\bullet+}$-AlPor-$C_{60}^{\bullet-}$ compared to $AlPor^{\bullet+}$-$C_{60}^{\bullet-}$ should stabilize the charge separation. A comparison of time profiles of $C_{60}^{\bullet-}$ for AlPor-Ph-C_{60} and BTMPA-Im→AlPor-Ph-C_{60} is shown in the Figure 7b. As can be seen, the two traces are virtually identical except for the rise time which is slightly shorter for the triad and a slight difference beyond 2000 ps suggesting that the decay of $C_{60}^{\bullet-}$ in the triad (blue trace) may be slightly slower than in the dyad (red trace). The fact that the two traces are essentially identical up to ~2000 ps suggests that if hole transfer involving BTMPA occurs in this triad it is slow.

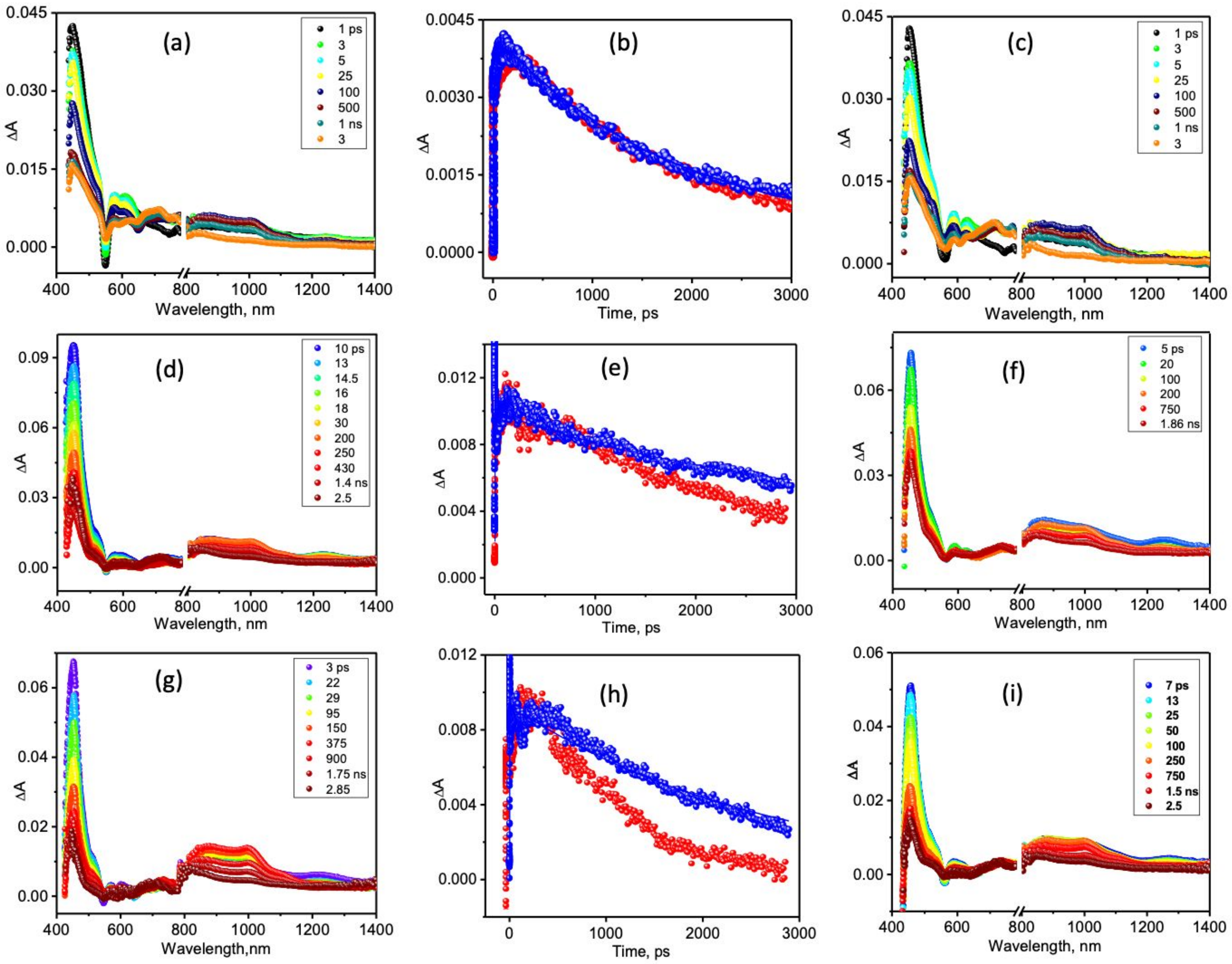

Figure 7. Femtosecond transient absorption spectra at the indicated delay times (λ_{ex} = 410 nm) of (a) AlPor-Ph-C_{60}, (c) BTMPA-Im→AlPor-Ph-C_{60}, (d) $AlPorF_3$-Ph-C_{60}, (f) BTMPA-Im→$AlPorF_3$-Ph-C_{60}, (g) $AlPorF_5$-Ph-C_{60}, and (i) BTMPA-Im→$AlPorF_5$-Ph-C_{60} in toluene. The central panels (b), (e) and (h) shows time profile of the $C_{60}^{\bullet-}$ peak in the absence (red trace) and presence (blue trace) of coordinated BTMPA to a given $AlPorF_n$-Ph-C_{60}.

For the triads BTMPA-Im→AlPorF$_3$-Ph-C$_{60}$ and BTMPA-Im→AlPorF$_5$-Ph-C$_{60}$, the energy level diagrams shown in Figure 4 predict that the hole transfer process is exothermic by 0.37 eV and 0.54 eV, respectively, which is considerably more favorable than in BTMPA-Im→AlPor-Ph-C$_{60}$. Consistent with this, the effect of hole transfer process further stabilizing the final charge separated states is clearly visible in the femtosecond transient absorbance data. Figures 7d and g show the transient absorption spectra at selected delay time and in both dyads, evidence for charge separation from the excited singlet state of the porphyrin leading to the formation of AlPorF$_3^{\bullet+}$-C$_{60}^{\bullet-}$ and AlPorF$_5^{\bullet+}$-C$_{60}^{\bullet-}$ is seen. The values of k_{CS} were determined by fitting the decay of the 1230 nm peak corresponding to singlet-singlet absorption of ^{1}AlPorF$_3^*$ and ^{1}AlPorF$_5$* and are listed in Table 3. As shown in the middle panels of Figure 7e and h, the decay of the C$_{60}^{\bullet-}$ peak (red traces) lasted beyond 3 ns (red trace), similar to that observed for AlPor-Ph-C$_{60}$ dyad. For BTMPA-Im→AlPorF$_3$-Ph-C$_{60}$ and BTMPA-Im→AlPorF$_5$-Ph-C$_{60}$ (Figures 7f and i) similar k_{CS} values are obtained (see Table 3). The comparisons of the time profiles of the C$_{60}^{\bullet-}$ peak of the triads (blue traces) dyads (red traces) show that the decay is significantly slower in the triads and is slowest in BTMPA-Im→AlPorF$_5$-Ph-C$_{60}$. This suggests that the decay of C$_{60}^{\bullet-}$ competes with hole transfer from BTMPA and that rate of hole transfer is faster BTMPA-Im→AlPorF$_5$-Ph-C$_{60}$ as expected from the larger driving force and lower activation energy.

Table 3. Rate constants for charge separation, k_{CS} and charge recombination, k_{CR} and overall lifetime of the radical ion-pair, τ_{RIP} evaluated from femto- and nanosecond transient absorption spectroscopy for the investigated dyads and triads in toluene.

Compound	k_{CS}, x 10^9 (s^{-1})	k_{CR}, x 10^6 (s^{-1})	τ_{RIP} (μs)	Ref
TMPA-Im →AlPor-Ph	--	--	--	tw
TMPA-Im →AlPorF$_3$-Ph	0.80	--	--	tw
TMPAIm →AlPorF$_5$-Ph	1.83	--	--	tw
AlPor-Ph-C$_{60}$	6.45	26.3	0.038	[66]
AlPorF$_3$-Ph-C$_{60}$	2.52	1.85	0.54	tw
AlPorF$_5$-Ph-C$_{60}$	4.27	1.51	0.66	tw
TMPA-Im →AlPor-Ph-C$_{60}$	2.53	17.9	0.056	tw
TMPA-Im →AlPorF$_3$-Ph-C$_{60}$	1.21	1.35	0.74	tw
TMPA-Im →AlPorF$_5$-Ph-C$_{60}$	3.44	0.81	1.24	tw

tw = this work

Nanosecond Transient Absorption Spectroscopy.

Lastly, to evaluate the lifetime of the final charge-separated states, nanosecond transient spectral measurements were performed on all of the newly assembled systems and the data are shown in Figure 8. Although relatively weak, in all of the dyads and triads, the C$_{60}^{\bullet-}$ peak at ~1000 nm could be observed indicating persistence of the radical ion-pair into the nanosecond to microsecond time window. In addition to peaks of C$_{60}^{\bullet-}$, transient features in the 460 and 850 nm range corresponding to ^{3}AlPorF$_n$* and in the 700 nm range corresponding to ^{3}C$_{60}$* were also observed. These results suggest that the singlet excited AlPorF$_n$ and/or the charge-separated species could competitively populate the triplet excited states to some extent. The lifetime of the absorbance changes at 1000 nm due to $C_{60}^{\bullet-}$ was used to calculate k_{CR} and lifetime of the radical ion-pairs.

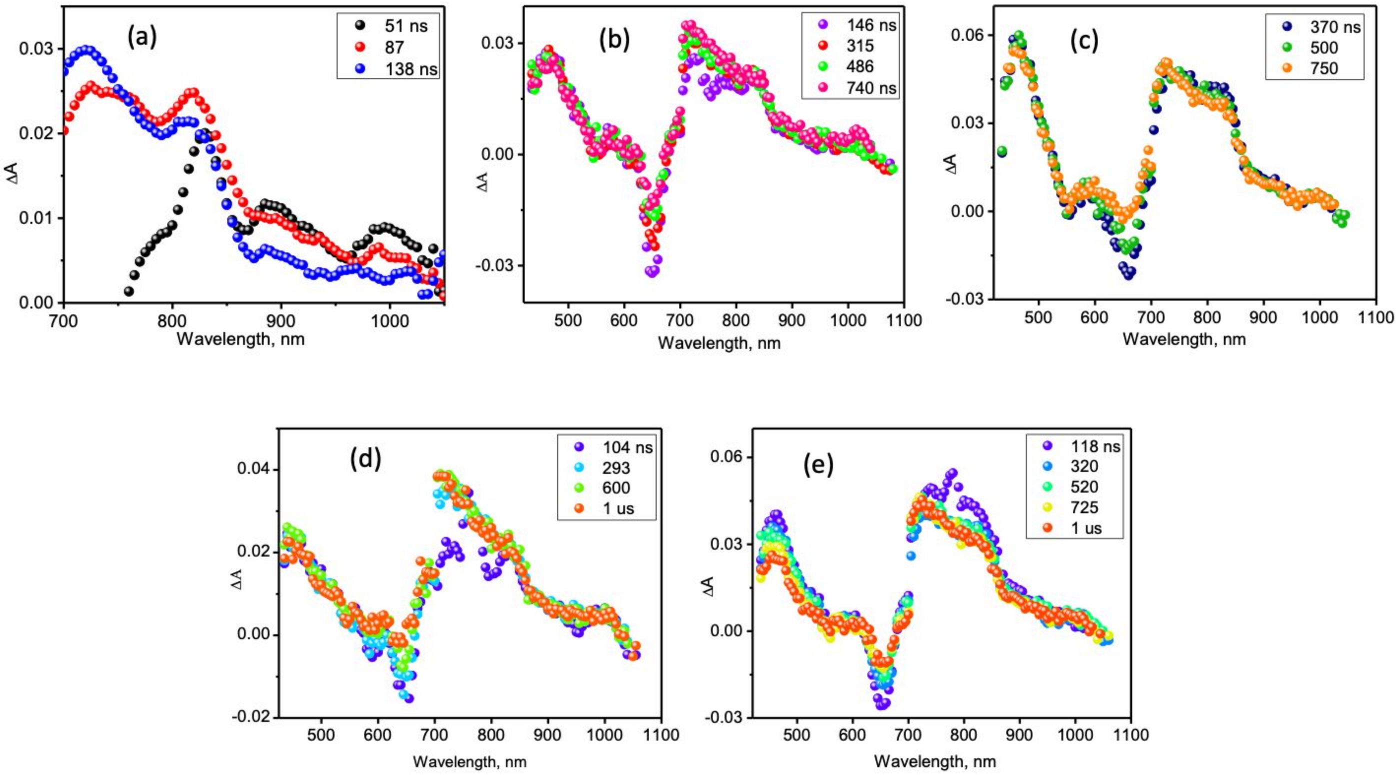

Figure 8. Nanosecond transient absorption spectra at the indicated delay times (λ_{ex} = 410 nm) of (a) BTMPA-Im→AlPor-Ph-C_{60}, (b) AlPorF$_3$-Ph-C_{60}, (c) BTMPA-Im→AlPorF$_3$-Ph-C_{60}, (d) AlPorF$_5$-Ph-C_{60}, and (e) BTMPA-Im→AlPorF$_5$-Ph-C_{60} in toluene.

The data listed in Table 3 reveal several features. (i) The rates of hole transfer from ^{1}AlPorF$_n$* to coordinated BTMPA are lower than those of electron transfer from ^{1}AlPorF$_n$* to C_{60}. Thus, we surmise that in the triads, electron transfer from the excited singlet state of AlPorF$_n$ to C_{60} occurs first and subsequently a hole transfer from AlPorF$_n^{\bullet+}$ to BTMPA takes place. (ii) Generally, the rate constant for charge separation k_{CS} correlates with the free-energy difference between the excited singlet state of the porphyrin and the charge-separated state AlPor$^{\bullet+}$-$C_{60}^{\bullet-}$, that is, a higher rate constant is observed for AlPor-Ph-C_{60} compared to the dyads with the fluorinated AlPorF$_3$-Ph-C_{60} and AlPorF$_5$-Ph-C_{60}. (iii) Coordination of BTMPA causes a slight increase in k_{CS}. A possible explanation for this is that coordination of BTMPA-Im to AlPorF$_n$ draws the porphyrin ring slightly closer to the C_{60} unit by pulling the Al center into the porphyrin plane as suggested by DFT studies. (iv) Finally, the k_{CR} values decrease (τ_{RIP} values increase) with increasing fluorination of porphyrin for both the dyads and triads. This is especially intriguing considering the fact that the final charge separated state in the triads is the same and has the same energy (1.50 eV). These results suggest that the central electron deficient AlPorF$_3$ or AlPorF$_5$ plays a key role in slowing down the charge recombination process.

Recombination mechanism and lifetimes. The lifetimes of the charge-separated states $AlPorF_n^{\bullet+}-C_{60}^{\bullet-}$ in the dyads can be rationalized by using the Marcus equation (3)[85–87] to relate the driving force (ΔG_{ET}) to the rate constants (k_{ET}) of the charge separation or charge recombination. Here, λ is the reorganization energy, V is the electronic coupling matrix element, k_B is the Boltzmann constant, h is the Planck constant, and T is the absolute temperature.

$$k_{ET} = \left(\frac{4\pi^3}{h^2\lambda k_B T}\right)^{\frac{1}{2}} V^2 exp\left[-\frac{(\Delta G_{ET} + \lambda)^2}{4\lambda k_B T}\right] \tag{3}$$

The values of 38, 540 and 660 ns for τ_{CR} in the dyads AlPor-Ph-C_{60}, $AlPorF_3$-Ph-C_{60} and $AlPorF_5$-Ph-C_{60}, respectively, clearly show that the radical pair is stabilized by substitution of fluorine atoms on the phenyl substituents of the porphyrin ring. This is because the corresponding driving force for recombination, (ΔG_{ET} = –1.50, –1.87, –2.04 eV) places the recombination far into the Marcus inverted region if the reorganization energy, λ, is on the order of 0.2 eV as suggested from studies of other porphyrin fullerene dyads.[31] Therefore, the charge recombination becomes slower as the driving force for recombination increases. It is important to compare these results with some related systems in the literature. For example, the charge separation and recombination in "axial-bonding" type high potential zinc(II) porphyrin – C_{60} dyads have been studied as a function of driving force.[88] However, the recombination rates did not follow the expected trend and the highly fluorinated zinc(II) porphyrin – C_{60} dyads showed faster recombination than the non-fluorinated zinc(II) porphyrin-C_{60} dyad. This suggests that either the electronic coupling or the recombination pathway differed in the different dyads. Numerous "horizontal" zinc(II) porphyrin – C_{60} dyad compounds have also been reported in the literature.[26,28] In these systems, the charge recombination sometimes occurs to the C_{60} triplet state[28] depending on the nature of the bridging groups and energy of the charge separated state. For those in which direct recombination to the ground state occurs, the rates are typically slower than observed here, suggesting that the electronic coupling is larger in the vertical arrangement.[26]

Unlike the dyads, all of the investigated triads produce the same radical pair, $BTMPA^{\bullet+}-AlPorF_n-C_{60}^{\bullet-}$, with an identical energy of 1.50 eV but with a significant difference in their lifetimes. We note, however, that value of the energy is based on the midpoint potential of unbound BTMPA and some small variation in the energies of the final radical pairs is expected. Nonetheless, the observed lifetime differences are too large to be reasonably explained using the free energy differences (ΔG) or different reorganization energies (λ) of the final radical pair. Instead, factors such as the electronic coupling (V) and/or a hopping/superexchange mechanism must be invoked to explain the variation in the backreaction rates. In the case of BTMPA-Im→AlPor-Ph-C_{60}, the final radical pair lifetime was found to be 56 ns and is only slightly longer than the 38 ns observed for the corresponding dyad. The DFT calculations revealed that strong electronic coupling exists between the AlPor and BTMPA units as the HOMO and HOMO-1 are delocalized significantly onto the BTMPA and AlPor, respectively. Moreover, the estimated energies of the AlPor$^{•+}$-$C_{60}^{•−}$, and BTMPA$^{•+}$-AlPor-$C_{60}^{•−}$ are identical. Under these conditions, it is likely that if the radical pair BTMPA$^{•+}$-AlPor-$C_{60}^{•−}$ is formed, its recombination to AlPor$^{•+}$-$C_{60}^{•−}$ probably has a lifetime that is similar to that of the decay of AlPor$^{•+}$-$C_{60}^{•−}$ to the ground state. In an incoherent hopping mechanism, this would result in a lifetime for the BTMPA$^{•+}$-AlPor-$C_{60}^{•−}$ radical pair that is similar to that of AlPor$^{•+}$-$C_{60}^{•−}$ in the dyad. In contrast, for BTMPA-Im→AlPorF$_3$-Ph-C_{60}, a hopping mechanism is unlikely because the electronic coupling between AlPorF$_3$ and BTMPA is weaker and the possible intermediates AlPor$^{•+}$-$C_{60}^{•−}$ and BTMPA$^{•+}$-AlPorF$_3^{•−}$ radical pairs are much higher in energy than the final radical pair BTMPA$^{•+}$-AlPorF$_3$-$C_{60}^{•−}$. Thus, the lifetime of 740 ns probably represents direct recombination to the ground state and is an order of magnitude longer than that of BTMPA$^{•+}$-AlPor-$C_{60}^{•−}$. Similarly, in the triad BTMPA-Im→AlPorF$_5$-Ph-C_{60}, the final radical pair also likely decays directly to the ground state because of the high energies of the possible intermediate radical pairs and weak electronic coupling. The lifetime of 1240 ns of the final radical pair BTMPA$^{•+}$-AlPorF$_5$-$C_{60}^{•−}$ is slightly longer than that of BTMPA$^{•+}$-AlPorF$_3$-$C_{60}^{•−}$ suggesting that either there is a small difference in the electronic coupling or the electron withdrawing effect of the porphyrin substituents leads to a small stabilization of BTMPA$^{•+}$-AlPorF$_5$-$C_{60}^{•−}$ in the triad. Thus, the fact that the recombination lifetime is different for the triads BTMPA-Im→AlPorF$_3$-Ph-C_{60} and BTMPA-Im→AlPorF$_5$-Ph-C_{60} indicates that the central porphyrin (AlPorF$_3$ *vs* AlPorF$_5$) is important in determining the lifetime of the charge separation because it has an impact on the energies of possible recombination intermediates and therefore on the possible recombination mechanisms.

CONCLUSION

The triads studied here are related to other axial-bonding triads we have reported previously [35,63–67] with a general formula of "Donor-Py/Im→Al(III)Porphyrin-Acceptor". A variety of donor and acceptor units have been employed and in all of these systems, sequential electron transfer takes place resulting in stable charge separation between the donor and acceptor. By varying the components of triads we have been able to study the sequential charge separation and recombination processes as a function of factors such as the donor-acceptor distance,[35] reorganization energy,[89,90] Gibbs free-energy,[64] and solvent polarity.[67] The observed charge recombination lifetimes can be rationalized using the Marcus equation and both the superexchange mechanism and incoherent electron transfer have been invoked to explain the recombination rates.

Previously, the focus has been on varying the terminal redox units or bridging groups to study their effect on the charge separation and recombination rates. Although these studies provide insight into the relationship between the components of the complexes and the rates, it is sometimes unclear which variable is responsible for observed differences in the rates. Here, by keeping the terminal redox units constant and making as small a structural change as possible to the central porphyrin to change its redox potential, it is possible to keep some of the electron transfer factors fixed, such as the distance and bridge between redox/photoactive active units, reorganization energy, free energy of the final charge separated state, etc. As a result, the observed changes in the rates can be clearly ascribed to the changes in the redox potential of the porphyrin. Similar triads but with the donor and acceptor attached in the plane of the porphyrin have also been reported Imahori and co-workers[26,78] but in these systems, the central metal of the porphyrin was altered to change its redox potential. In contrast, to the systems reported here, in which the recombination reaction is far into the Marcus inverted region, the recombination reaction was close to the top of the Marcus curve and the back reaction rate was governed primarily by the electronic coupling which was much smaller due to the different bonding arrangement. From this comparison, it is clear that these two factors must be balanced against each other to achieve long-lived charge separation. In systems, like the ones presented here in which the electronic coupling is fairly strong, it is important that the back reaction should lie far into the Marcus inverted region. This means that the midpoint potential of the central porphyrin should be chosen so that possible intermediates in a hopping mechanism of charge recombination are high enough in energy to make them inaccessible.

ASSOCIATED CONTENT

Supporting Information: Synthesis schemes and details**,** spectroscopic experiments, mass, IR and NMR spectra, absorption spectra, binding constants, spectroscopic titrations, phosphorescence spectra, DFT optimized structures with frontier orbitals, energy level diagram in *o*-DCB, and spectroelectrochemical data.

AUTHOR INFORMATION

Corresponding authors.

Prashanth K. Poddutoori. *Department of Chemistry & Biochemistry, University of Minnesota Duluth, 1038 University Drive, Duluth, Minnesota 55812, United States.* Email: ppk@d.umn.edu

Francis D'Souza. *Department of Chemistry, University of North Texas, 1155 Union Circle, # 305070, Denton, Texas 76203-5017, United States*. Email: francis.dsouza@unt.edu

Art van der Est. *Department of Chemistry, Brock University, 1812 Sir Isaac Brock Way, St. Catharines, ON, L2S 3A1, Canada.* Email: avde@brocku.ca

Victor S. Batista. *Department of Chemistry, Yale University, P.O. Box 208107, New Haven, Connecticut 06520-8107, United States*. Email: victor.batista@yale.edu

Authors.

Niloofar Zarrabi. *Department of Chemistry & Biochemistry, University of Minnesota Duluth, 1038 University Drive, Duluth, Minnesota 55812, United States.*

Sairaman Seetharaman. *Department of Chemistry, University of North Texas, 1155 Union Circle, # 305070, Denton, Texas 76203-5017, United States.*

Subhajyoti Chaudhuri. *Department of Chemistry, Yale University, P.O. Box 208107, New Haven, Connecticut 06520-8107, United States.*

Noah Holzer. *Department of Chemistry & Biochemistry, University of Minnesota Duluth, 1038 University Drive, Duluth, Minnesota 55812, United States.*

Notes. The authors declare no competing financial interest.

ACKNOWLEDGEMENTS.

This work was supported by startup grants from the University of Minnesota Duluth, to PPK, and by the National Science Foundation (Grant No. 1401188) to FD and by an NSERC Discovery Grant (2015-04021) to AvdE.

REFERENCES.

(1) Barber, J.; Andersson, B. Revealing the Blueprint of Photosynthesis. *Nature* **1994**, *370* (6484), 31–34. https://doi.org/10.1038/370031a0.

(2) Blankenship, R. E. *Molecular Mechanisms of Photosynthesis*; 2008. https://doi.org/10.1002/9780470758472.

(3) Deisenhofer, J.; Norris, J. R. *Photosynthetic Reaction Center, Two-Volume Set: Photosynthetic Reaction Center, Volume 2*; Academic Press: San Diego, CA, 1993.

(4) Hou, H. J. M.; Najafpour, M. M.; Moore, G. F.; Allakhverdiev, S. I. *Photosynthesis: Structures, Mechanisms, and Applications*; Springer, Cham, 2017. https://doi.org/10.1007/978-3-319-48873-8.

(5) Barber, J. Photosynthetic Energy Conversion: Natural and Artificial. *Chem. Soc. Rev.* **2009**, *38* (1), 185–196. https://doi.org/10.1039/b802262n.

(6) Fukuzumi, S. Development of Bioinspired Artificial Photosynthetic Systems. *Physical Chemistry Chemical Physics*. 2008, pp 2283–2297. https://doi.org/10.1039/b801198m.

(7) Hambourger, M.; Moore, G. F.; Kramer, D. M.; Gust, D.; Moore, A. L.; Moore, T. A. Biology and Technology for Photochemical Fuel Production. *Chem. Soc. Rev.* **2009**, *38* (1), 25–35. https://doi.org/10.1039/b800582f.

(8) Armaroli, N.; Balzani, V. Solar Electricity and Solar Fuels: Status and Perspectives in the Context of the Energy Transition. *Chemistry - A European Journal*. 2016, pp 32–57. https://doi.org/10.1002/chem.201503580.

(9) Fukuzumi, S.; Ohkubo, K.; Suenobu, T. Long-Lived Charge Separation and Applications in Artificial Photosynthesis. *Acc. Chem. Res.* **2014**, *47* (5), 1455–1464. https://doi.org/10.1021/ar400200u.

(10) Imahori, H.; Mori, Y.; Matano, Y. Nanostructured Artificial Photosynthesis. *Journal of Photochemistry and Photobiology C: Photochemistry Reviews*. 2003, pp 51–83. https://doi.org/10.1016/S1389-5567(03)00004-2.

(11) El-Khouly, M. E.; El-Mohsnawy, E.; Fukuzumi, S. Solar Energy Conversion: From Natural to Artificial Photosynthesis. *Journal of Photochemistry and Photobiology C: Photochemistry Reviews*. 2017, pp 36–83. https://doi.org/10.1016/j.jphotochemrev.2017.02.001.

(12) Nocera, D. G. The Artificial Leaf. *Acc. Chem. Res.* **2012**, *45* (5), 767–776. https://doi.org/10.1021/ar2003013.

(13) Kurumisawa, Y.; Higashino, T.; Nimura, S.; Tsuji, Y.; Iiyama, H.; Imahori, H. Renaissance of Fused Porphyrins: Substituted Methylene-Bridged Thiophene-Fused Strategy for High-Performance Dye-

Sensitized Solar Cells. *J. Am. Chem. Soc.* **2019,** *141*(25), 9910-9919. https://doi.org/10.1021/jacs.9b03302.

(14) Yamamoto, M.; Föhlinger, J.; Petersson, J.; Hammarström, L.; Imahori, H. A Ruthenium Complex–Porphyrin–Fullerene-Linked Molecular Pentad as an Integrative Photosynthetic Model. *Angew. Chemie - Int. Ed.* **2017**, *56* (12), 3329–3333. https://doi.org/10.1002/anie.201612456.

(15) Fukuzumi, S.; Lee, Y. M.; Nam, W. Bioinspired Artificial Photosynthesis Systems. *Tetrahedron* **2020**, *76*. https://doi.org/10.1016/j.tet.2020.131024.

(16) Sampaio, R. N.; Troian-Gautier, L.; Meyer, G. J. A Charge-Separated State That Lives for Almost a Second at a Conductive Metal Oxide Interface. *Angew. Chemie - Int. Ed.* **2018**, *57* (47), 15390–15394. https://doi.org/10.1002/anie.201807627.

(17) Whang, D. R.; Apaydin, D. H. Artificial Photosynthesis: Learning from Nature. *ChemPhotoChem* **2018**, *2* (3), 148–160. https://doi.org/10.1002/cptc.201700163.

(18) Guldi, D. M. Fullerene-Porphyrin Architectures; Photosynthetic Antenna and Reaction Center Models. *Chem. Soc. Rev.* **2002**, *31* (1), 22–36. https://doi.org/10.1039/b106962b.

(19) Gust, D.; Moore, T. A.; Moore, A. L. Mimicking Photosynthetic Solar Energy Transduction. *Acc. Chem. Res.* **2001**, *34* (1), 40–48. https://doi.org/10.1021/ar9801301.

(20) Kodis, G.; Terazono, Y.; Liddell, P. A.; Andréasson, J.; Garg, V.; Hambourger, M.; Moore, T. A.; Moore, A. L.; Gust, D. Energy and Photoinduced Electron Transfer in a Wheel-Shaped Artificial Photosynthetic Antenna-Reaction Center Complex. *J. Am. Chem. Soc.* **2006**, *128* (6), 1818–1827. https://doi.org/10.1021/ja055903c.

(21) Kuramochi, Y.; Sandanayaka, A. S. D.; Satake, A.; Araki, Y.; Ogawa, K.; Ito, O.; Kobuke, Y. Energy Transfer Followed by Electron Transfer in a Porphyrin Macrocycle and Central Acceptor Ligand: A Model for a Photosynthetic Composite of the Light-Harvesting Complex and Reaction Center. *Chem. - A Eur. J.* **2009**, *15* (10), 2317–2327. https://doi.org/10.1002/chem.200801796.

(22) Gust, D.; Moore, T. A.; Moore, A. L. Solar Fuels via Artificial Photosynthesis. *Acc. Chem. Res.* **2009**, *42* (12), 1890–1898. https://doi.org/10.1021/ar900209b.

(23) Wasielewski, M. R. Self-Assembly Strategies for Integrating Light Harvesting and Charge Separation in Artificial Photosynthetic Systems. *Acc. Chem. Res.* **2009**, *42* (12), 1910–1921. https://doi.org/10.1021/ar9001735.

(24) Fiechter, S. Artificial Photosynthesis - An Inorganic Approach. *Adv. Bot. Res.* **2016**, *79*, 99–128. https://doi.org/10.1016/bs.abr.2016.04.002.

(25) Gust, D. An Illustrative History of Artificial Photosynthesis. *Adv. Bot. Res.* **2016**, *79*, 1–42. https://doi.org/10.1016/bs.abr.2016.02.004.

(26) Imahori, H.; Tamaki, K.; Guldi, D. M.; Luo, C.; Fujitsuka, M.; Ito, O.; Sakata, Y.; Fukuzumi, S. Modulating Charge Separation and Charge Recombination Dynamics in Porphyrin-Fullerene Linked Dyads and Triads: Marcus-Normal versus Inverted Region. *J. Am. Chem. Soc.* **2001**, *123* (11), 2607–2617. https://doi.org/10.1021/ja003346i.

(27) Schuster, D. I.; Cheng, P.; Jarowski, P. D.; Guldi, D. M.; Luo, C.; Echegoyen, L.; Pyo, S.; Holzwarth, A. R.; Braslavsky, S. E.; Williams, R. M.; Klihm, G. Design, Synthesis, and Photophysical Studies of a Porphyrin-Fullerene Dyad with Parachute Topology; Charge Recombination in the Marcus Inverted Region. *J. Am. Chem. Soc.* **2004**, *126* (23), 7257–7270. https://doi.org/10.1021/ja038676s.

(28) Wolf, M.; Costa, J. I. T.; Minameyer, M. B.; Drewello, T.; Tomé, A. C.; Guldi, D. M. Efficient Low Driving Force Charge Separation in an Electron Deficient Zn-Porphyrin-Fullerene Donor-Acceptor Conjugate. *J. Phys. Chem. C* **2019**, *123* (46), 28093–28099. https://doi.org/10.1021/acs.jpcc.9b09790.

(29) Imahori, H.; Yamada, H.; Guldi, D. M.; Endo, Y.; Shimomura, A.; Kundu, S.; Yamada, K.; Okada, T.; Sakata, Y.; Fukuzumi, S. Comparison of Reorganization Energies for Intra- and Intermolecular Electron Transfer. *Angew. Chemie - Int. Ed.* **2002**, *41* (13), 2344–2347. https://doi.org/10.1002/1521-3773(20020703)41:13<2344::AID-ANIE2344>3.0.CO;2-7.

(30) Stangel, C.; Schubert, C.; Kuhri, S.; Rotas, G.; Margraf, J. T.; Regulska, E.; Clark, T.; Torres, T.; Tagmatarchis, N.; Coutsolelos, A. G.; Guldi, D. M. Tuning the Reorganization Energy of Electron Transfer in Supramolecular Ensembles - Metalloporphyrin, Oligophenylenevinylenes, and Fullerene -

And the Impact on Electron Transfer Kinetics. *Nanoscale* **2015**, *7* (6), 2597–2608. https://doi.org/10.1039/c4nr05165c.

(31) Imahori, H.; Tkachenko, N. V.; Vehmahen, V.; Tamaki, K.; Lemmetyinen, H.; Sakata, Y.; Fukuzumi, S. An Extremely Small Reorganization Energy of Electron Transfer in Porphyrin-Fullerene Dyad. *J. Phys. Chem. A* **2001**, *105* (10), 1750–1756. https://doi.org/10.1021/jp003207n.

(32) Guldi, D. M.; Hirsch, A.; Scheloske, M.; Dietel, E.; Troisi, A.; Zerbetto, F.; Prato, M. Modulating Charge-Transfer Interactions in Topologically Different Porphyrin-C60 Dyads. *Chem. - A Eur. J.* **2003**, *9* (20), 4968–4979. https://doi.org/10.1002/chem.200304995.

(33) Di Valentin, M.; Bisol, A.; Agostini, G.; Carbonera, D. Electronic Coupling Effects on Photoinduced Electron Transfer in Carotene - Porphyrin-Fullerene Triads Detected by Time-Resolved EPR. In *Journal of Chemical Information and Modeling*; 2005; Vol. 45, pp 1580–1588. https://doi.org/10.1021/ci050183e.

(34) Higashino, T.; Yamada, T.; Yamamoto, M.; Furube, A.; Tkachenko, N. V.; Miura, T.; Kobori, Y.; Jono, R.; Yamashita, K.; Imahori, H. Remarkable Dependence of the Final Charge Separation Efficiency on the Donor-Acceptor Interaction in Photoinduced Electron Transfer. *Angew. Chemie - Int. Ed.* **2016**, *55* (2), 629–633. https://doi.org/10.1002/anie.201509067.

(35) Poddutoori, P. K.; Lim, G. N.; Sandanayaka, A. S. D.; Karr, P. A.; Ito, O.; D'Souza, F.; Pilkington, M.; Van Der Est, A. Axially Assembled Photosynthetic Reaction Center Mimics Composed of Tetrathiafulvalene, Aluminum(Iii) Porphyrin and Fullerene Entities. *Nanoscale* **2015**, *7* (28), 12151–12165. https://doi.org/10.1039/c5nr01675d.

(36) Weiss, E. A.; Ahrens, M. J.; Sinks, L. E.; Gusev, A. V.; Ratner, M. A.; Wasielewski, M. R. Making a Molecular Wire: Charge and Spin Transport through Para-Phenylene Oligomers. *J. Am. Chem. Soc.* **2004**, *126* (17), 5577–5584. https://doi.org/10.1021/ja0398215.

(37) Schubert, C.; Margraf, J. T.; Clark, T.; Guldi, D. M. Molecular Wires-Impact of π-Conjugation and Implementation of Molecular Bottlenecks. *Chem. Soc. Rev.* **2015**, *44* (4), 988–998. https://doi.org/10.1039/c4cs00262h.

(38) Gilbert, M.; Albinsson, B. Photoinduced Charge and Energy Transfer in Molecular Wires. *Chemical Society Reviews*. 2015, pp 845–862. https://doi.org/10.1039/c4cs00221k.

(39) Ito, O.; Yamanaka, K. I. Roles of Molecular Wires between Fullerenes and Electron Donors in Photoinduced Electron Transfer. *Bull. Chem. Soc. Jpn.* **2009**, *82* (3), 316–332. https://doi.org/10.1246/bcsj.82.316.

(40) Benniston, A. C.; Harriman, A. Charge on the Move: How Electron-Transfer Dynamics Depend on Molecular Conformation. *Chemical Society Reviews*. 2006, pp 169–179. https://doi.org/10.1039/b503169a.

(41) Guldi, D. M.; Imahori, H.; Tamaki, K.; Kashiwagi, Y.; Yamada, H.; Sakata, Y.; Fukuzumi, S. A Molecular Tetrad Allowing Efficient Energy Storage for 1.6 s at 163 K. *J. Phys. Chem. A* **2004**, *108* (4), 541–548. https://doi.org/10.1021/jp036382n.

(42) Imahori, H.; Guldi, D. M.; Tamaki, K.; Yoshida, Y.; Luo, C.; Sakata, Y.; Fukuzumi, S. Charge Separation in a Novel Artificial Photosynthetic Reaction Center Lives 380 Ms. *J. Am. Chem. Soc.* **2001**, *123* (27), 6617–6628. https://doi.org/10.1021/ja004123v.

(43) Luo, C.; Guldi, D. M.; Imahori, H.; Tamaki, K.; Sakata, Y. Sequential Energy and Electron Transfer in an Artificial Reaction Center: Formation of a Long-Lived Charge-Separated State. *J. Am. Chem. Soc.* **2000**, *122* (28), 6535–6551. https://doi.org/10.1021/ja993959z.

(44) Lee, S. H.; Blake, I. M.; Larsen, A. G.; McDonald, J. A.; Ohkubo, K.; Fukuzumi, S.; Reimers, J. R.; Crossley, M. J. Synthetically Tuneable Biomimetic Artificial Photosynthetic Reaction Centres That Closely Resemble the Natural System in Purple Bacteria. *Chem. Sci.* **2016**, *7* (10), 6534–6550. https://doi.org/10.1039/c6sc01076h.

(45) Otsuki, J. Supramolecular Approach towards Light-Harvesting Materials Based on Porphyrins and Chlorophylls. *J. Mater. Chem. A* **2018**, *6* (16), 6710–6753. https://doi.org/10.1039/c7ta11274b.

(46) Kadish, K. M.; Smith, K. M.; Guilard, R. *The Porphyrin Handbook*; 2012; Vol. 11. https://doi.org/10.1016/C2009-0-22714-0.

(47) Fukuzumi, S.; Kashiwagi, Y. Photoinduced Electron Transfer in a Supramolecular Triad System

Composed of Ferrocene-Zinc Porphyrin-Pyridylnaphthalenediimide. *J. Porphyr. Phthalocyanines* **2007**, *11* (5–6), 368–374. https://doi.org/10.1142/s1088424607000412.

(48) Hyun, J. K.; Park, K. M.; Tae, K. A.; Seong, K. K.; Kil, S. K.; Kim, D.; Kim, H. J. Novel Fullerene-Porphyrin-Fullerene Triad Linked by Metal Axial Coordination: Synthesis, X-Ray Crystal Structure, and Spectroscopic Characterizations of Trans-Bis([60]Fullerenoacetato)Tin(IV) Porphyrin. *Chem. Commun.* **2004**, *10* (22), 2594–2595. https://doi.org/10.1039/b411482e.

(49) Zhan, Y.; Cao, K.; Wang, C.; Jia, J.; Xue, P.; Liu, X.; Duan, X.; Lu, R. Synthesis and Photophysical Properties of Phosphorus(v) Porphyrins Functionalized with Axial Carbazolylvinylnaphthalimides. *Org. Biomol. Chem.* **2012**, *10* (43), 8701–8709. https://doi.org/10.1039/c2ob26478a.

(50) Nagao, K.; Takeuchi, Y.; Segawa, H. Geometry and Solvent-Polarity Dependences of the Relaxation Dynamics of the Singlet Excited State of Center-to-Edge Phosphorus(V) Porphyrin Heterodimers. *J. Phys. Chem. B* **2006**, *110* (10), 5120–5126. https://doi.org/10.1021/jp044468q.

(51) Hirakawa, K.; Segawa, H. Effects of Hydrogen Bonding Interaction and Solvent Polarity on the Competition between Excitation Energy and Photo-Induced Electron Transfer Processes in Hydroxy(1-Pyrenebutoxy)Phosphorus(V)Porphyrin. *J. Photochem. Photobiol. A Chem.* **2010**, *213* (1), 73–79. https://doi.org/10.1016/j.jphotochem.2010.05.002.

(52) Giribabu, L.; Rao, T. A.; Maiya, B. G. “Axial-Bonding”-Type Hybrid Porphyrin Arrays: Synthesis, Spectroscopy, Electrochemistry, and Singlet State Properties. *Inorg. Chem.* **1999**, *38* (22), 4971–4980. https://doi.org/10.1021/ic990326c.

(53) D’Souza, F.; Ito, O. Photoinduced Electron Transfer in Supramolecular Systems of Fullerenes Functionalized with Ligands Capable of Binding to Zinc Porphyrins and Zinc Phthalocyanines. In *Coordination Chemistry Reviews*; 2005; Vol. 249, pp 1410–1422. https://doi.org/10.1016/j.ccr.2005.01.002.

(54) El-Khouly, M. E.; Ito, O.; Smith, P. M.; D’Souza, F. Intermolecular and Supramolecular Photoinduced Electron Transfer Processes of Fullerene-Porphyrin/Phthalocyanine Systems. *Journal of Photochemistry and Photobiology C: Photochemistry Reviews*. 2004, pp 79–104. https://doi.org/10.1016/j.jphotochemrev.2004.01.003.

(55) Iengo, E.; Pantosx, G. D.; Sanders, J. K. M.; Orlandi, M.; Chiorboli, C.; Fracassoc, S.; Scandola, F. A Fully Self-Assembled Non-Symmetric Triad for Photoinduced Charge Separation. *Chem. Sci.* **2011**, *2* (4), 676–685. https://doi.org/10.1039/c0sc00520g.

(56) Kanematsu, M.; Naumov, P.; Kojima, T.; Fukuzumi, S. Intermolecular and Intracomplex Photoinduced Electron Transfer from Planar and Nonplanar Metalloporphyrins to P-Quinones. *Chem. - A Eur. J.* **2011**, *17* (44), 12372–12384. https://doi.org/10.1002/chem.201100493.

(57) Iengo, E.; Cavigli, P.; Gamberoni, M.; Teresa Indelli, M. A Selective Metal-Mediated Approach for the Efficient Self-Assembling of Multi-Component Photoactive Systems. *Eur. J. Inorg. Chem.* **2014**, No. 2, 337–344. https://doi.org/10.1002/ejic.201300998.

(58) Amati, A.; Cavigli, P.; Kahnt, A.; Indelli, M. T.; Iengo, E. Self-Assembled Ruthenium(II)Porphyrin-Aluminium(III)Porphyrin-Fullerene Triad for Long-Lived Photoinduced Charge Separation. *J. Phys. Chem. A* **2017**, *121* (22), 4242–4252. https://doi.org/10.1021/acs.jpca.7b02973.

(59) Obondi, C. O.; Lim, G. N.; Jang, Y.; Patel, P.; Wilson, A. K.; Poddutoori, P. K.; D’Souza, F. Charge Stabilization in High-Potential Zinc Porphyrin-Fullerene via Axial Ligation of Tetrathiafulvalene. *J. Phys. Chem. C* **2018**, *122* (25), 13636–13647. https://doi.org/10.1021/acs.jpcc.8b00028.

(60) Nikolaou, V.; Charisiadis, A.; Stangel, C.; Charalambidis, G.; Coutsolelos, A. G. Porphyrinoid–Fullerene Hybrids as Candidates in Artificial Photosynthetic Schemes. *C — J. Carbon Res.* **2019**, *5* (3), 57. https://doi.org/10.3390/c5030057.

(61) Moser, C. C.; Keske, J. M.; Warncke, K.; Farid, R. S.; Dutton, P. L. Nature of Biological Electron Transfer. *Nature* **1992**, *355* (6363), 796–802. https://doi.org/10.1038/355796a0.

(62) Zarrabi, N.; Agatemor, C.; Lim, G. N.; Matula, A. J.; Bayard, B. J.; Batista, V. S.; D’Souza, F.; Poddutoori, P. K. High-Energy Charge-Separated States by Reductive Electron Transfer Followed by Electron Shift in the Tetraphenylethylene-Aluminum(III) Porphyrin-Fullerene Triad. *J. Phys. Chem. C* **2019**, *123* (1), 131–143. https://doi.org/10.1021/acs.jpcc.8b09500.

(63) Poddutoori, P. K.; Bregles, L. P.; Lim, G. N.; Boland, P.; Kerr, R. G.; D'Souza, F. Modulation of Energy Transfer into Sequential Electron Transfer upon Axial Coordination of Tetrathiafulvalene in an Aluminum(III) Porphyrin-Free-Base Porphyrin Dyad. *Inorg. Chem.* **2015**, *54* (17), 8482–8494. https://doi.org/10.1021/acs.inorgchem.5b01190.

(64) Zarrabi, N.; Obondi, C. O.; Lim, G. N.; Seetharaman, S.; Boe, B. G.; D'Souza, F.; Poddutoori, P. K. Charge-Separation in Panchromatic, Vertically Positioned Bis(Donor Styryl)BODIPY-Aluminum(Iii) Porphyrin-Fullerene Supramolecular Triads. *Nanoscale* **2018**, *10* (44), 20723–20739. https://doi.org/10.1039/c8nr06649c.

(65) Poddutoori, P. K.; Sandanayaka, A. S. D.; Hasobe, T.; Ito, O.; Van Est, A. Der. Photoinduced Charge Separation in a Ferrocene-Aluminum(III) Porphyrin-Fullerene Supramolecular Triad. *J. Phys. Chem. B* **2010**, *114* (45), 14348–14357. https://doi.org/10.1021/jp911937d.

(66) Poddutoori, P. K.; Sandanayaka, A. S. D.; Zarrabi, N.; Hasobe, T.; Ito, O.; Van Der Est, A. Sequential Charge Separation in Two Axially Linked Phenothiazine- Aluminum(III) Porphyrin-Fullerene Triads. *J. Phys. Chem. A* **2011**, *115* (5), 709–717. https://doi.org/10.1021/jp110156w.

(67) Poddutoori, P. K.; Zarrabi, N.; Moiseev, A. G.; Gumbau-Brisa, R.; Vassiliev, S.; Van Der Est, A. Long-Lived Charge Separation in Novel Axial Donor-Porphyrin-Acceptor Triads Based on Tetrathiafulvalene, Aluminum(III) Porphyrin and Naphthalenediimide. *Chem. - A Eur. J.* **2013**, *19* (9), 3148–3161. https://doi.org/10.1002/chem.201202995.

(68) Poddutoori, P. K.; Lim, G. N.; Vassiliev, S.; D'Souza, F. Ultrafast Charge Separation and Charge Stabilization in Axially Linked "tetrathiafulvalene-Aluminum(Iii) Porphyrin-Gold(Iii) Porphyrin" Reaction Center Mimics. *Phys. Chem. Chem. Phys.* **2015**, *17* (39), 26346–26358. https://doi.org/10.1039/c5cp04818d.

(69) Poddutoori, P. K.; Kandrashkin, Y. E.; Est, A. Van Der. A Transient EPR Study of Electron Transfer in Tetrathiafulvalene-Aluminum(III) Porphyrin-Anthraquinone Supramolecular Triads. *Zeitschrift fur Phys. Chemie* **2017**, *231* (2), 293–310. https://doi.org/10.1515/zpch-2016-0826.

(70) Bagaki, A.; Gobeze, H. B.; Charalambidis, G.; Charisiadis, A.; Stangel, C.; Nikolaou, V.; Stergiou, A.; Tagmatarchis, N.; D'Souza, F.; Coutsolelos, A. G. Axially Assembled Photosynthetic Antenna-Reaction Center Mimics Composed of Boron Dipyrromethenes, Aluminum Porphyrin, and Fullerene Derivatives. *Inorg. Chem.* **2017**, *56* (17), 10268–10280. https://doi.org/10.1021/acs.inorgchem.7b01050.

(71) Davidson, G. J. E.; Tong, L. H.; Raithby, P. R.; Sanders, J. K. M. Aluminium(III) Porphyrins as Supramolecular Building Blocks. *Chem. Commun.* **2006**, No. 29, 3087–3089. https://doi.org/10.1039/b605435h.

(72) Metselaar, G. A.; Sanders, J. K. M.; De Mendoza, J. A Self-Assembled Aluminium(Iii) Porphyrin Cyclic Trimer. *J. Chem. Soc. Dalt. Trans.* **2007**, No. 5, 588–590. https://doi.org/10.1039/b717017n.

(73) Davidson, G. J. E.; Lane, L. A.; Raithby, P. R.; Warren, J. E.; Robinson, C. V.; Sanders, J. K. M. Coordination Polymers Based on Aluminum(III) Porphyrins. *Inorg. Chem.* **2008**, *47* (19), 8721–8726. https://doi.org/10.1021/ic800587y.

(74) Poddutoori, P. K.; Poddutoori, P.; Maiya, B. G.; Prasad, T. K.; Kandrashkin, Y. E.; Vasil'ev, S.; Bruce, D.; Van Der Est, A. Redox Control of Photoinduced Electron Transfer in Axial Terpyridoxy Porphyrin Complexes. *Inorg. Chem.* **2008**, *47* (17), 7512–7522. https://doi.org/10.1021/ic702480m.

(75) Guldi, D. M. Fullerenes: Three Dimensional Electron Acceptor Materials. *Chemical Communications*. 2000, pp 321–327. https://doi.org/10.1039/a907807j.

(76) Imahori, H.; Hagiwara, K.; Akiyama, T.; Aoki, M.; Taniguchi, S.; Okada, T.; Shirakawa, M.; Sakata, Y. The Small Reorganization Energy of C60 in Electron Transfer. *Chem. Phys. Lett.* **1996**, *263* (3–4), 545–550.

(77) Martín, N.; Sánchez, L.; Illescas, B.; Pérez, I. C60-Based Electroactive Organofullerenes. *Chem. Rev.* **1998**, *98* (7), 2527–2547. https://doi.org/10.1021/cr9701039.

(78) Imahori, H. Porphyrin-Fullerene Linked Systems as Artificial Photosynthetic Mimics. *Organic and Biomolecular Chemistry*. 2004, pp 1425–1433. https://doi.org/10.1039/b403024a.

(79) Lim, G. N.; Hedström, S.; Jung, K. A.; Smith, P. A. D.; Batista, V. S.; D'Souza, F.; Van Der Est, A.; Poddutoori, P. K. Interfacial Electron Transfer Followed by Photooxidation in N,N-Bis(p-

Anisole)Aminopyridine-Aluminum(III) Porphyrin-Titanium(IV) Oxide Self-Assembled Photoanodes. *J. Phys. Chem. C* **2017**, *121* (27), 14484–14497. https://doi.org/10.1021/acs.jpcc.7b04197.

(80) Becke, A. D. Density-Functional Thermochemistry. III. The Role of Exact Exchange. *J. Chem. Phys.* **1993**, *98* (7), 5648–5652. https://doi.org/10.1063/1.464913.

(81) Weigend, F.; Ahlrichs, R. Balanced Basis Sets of Split Valence, Triple Zeta Valence and Quadruple Zeta Valence Quality for H to Rn: Design and Assessment of Accuracy. *Phys. Chem. Chem. Phys.* **2005**, *7* (18), 3297–3305. https://doi.org/10.1039/b508541a.

(82) Robert, M. [Oxygen Affinity of Haemoglobin (Author’s Transl)]. *Bull. Physiopathol. Respir. (Nancy).* **2016**, *11* (1), 79–170. https://doi.org/111.

(83) Cossi, M.; Rega, N.; Scalmani, G.; Barone, V. Energies, Structures, and Electronic Properties of Molecules in Solution with the C-PCM Solvation Model. *J. Comput. Chem.* **2003**, *24* (6), 669–681. https://doi.org/10.1002/jcc.10189.

(84) Arbogast, J. W.; Darmanyan, A. P.; Foote, C. S.; Rubin, Y.; Diederich, F. N.; Alvarez, M. M.; Anz, S. J.; Whetten, R. L. Photophysical Properties of C60. *J. Phys. Chem.* **1991**, *95* (1), 11–12.

(85) Winkler, J. R.; Gray, H. B. Electron Transfer in Ruthenium-Modified Proteins. *Chem. Rev.* **1992**, *92* (3), 369–379. https://doi.org/10.1021/cr00011a001.

(86) McLendon, G. Long-Distance Electron Transfer in Proteins and Model Systems. *Acc. Chem. Res.* **1988**, *21* (4), 160–167. https://doi.org/10.1021/ar00148a005.

(87) Marcus, R. A. Electron Transfer Reactions in Chemistry. Theory and Experiment. *Rev. Mod. Phys.* **1993**, *65* (3), 599–610. https://doi.org/10.1103/RevModPhys.65.599.

(88) Das, S. K.; Song, B.; Mahler, A.; Nesterov, V. N.; Wilson, A. K.; Ito, O.; D’Souza, F. Electron Transfer Studies of High Potential Zinc Porphyrin-Fullerene Supramolecular Dyads. *J. Phys. Chem. C* **2014**, *118* (8), 3994–4006. https://doi.org/10.1021/jp4118166.

(89) Kandrashkin, Y. E.; Poddutoori, P. K.; van der Est, A. Electron Transfer Pathways in a Tetrathiafulvalene-Aluminum(III) Porphyrin-Free-Base Porphyrin Triad Studied Using Electron Spin Polarization. *Appl. Magn. Reson.* **2016**, *47* (5), 511–526. https://doi.org/10.1007/s00723-016-0774-8.

(90) van der Est, A.; Poddutoori, P. K. Light-Induced Spin Polarization in Porphyrin-Based Donor-Acceptor Dyads and Triads. *Appl. Magn. Reson.* **2013**, *44* (1–2), 301–318. https://doi.org/10.1007/s00723-012-0420-z.

Graphical Abstract:

Decelerating Charge Recombination Using Fluorinated Porphyrins in *N*,*N*-bis(3,4,5-trimethoxyphenyl)aniline – Aluminum(III) Porphyrin – Fullerene Reaction Center Models

Niloofar Zarrabi, Sairaman Seetharaman, Subhajyoti Chaudhuri, Noah Holzer, Victor S. Batista, Art van der Est,* Francis D'Souza,* Prashanth K. Poddutoori**